UNIVERSITY OF CALIFORNIA
RIVERSIDE

Synthesis of Molybdenum Oxide Nanostructures by Using the Laser Ablation of Solids in Liquids Technique

A Dissertation submitted in partial satisfaction
of the requirements for the degree of

Doctor of Philosophy

in

Materials Science and Engineering

by

Noe Zamora-Romero

December 2019

Dissertation Committee:
Dr. Guillermo Aguilar, Chairperson
Dr. Lorenzo Mangolini
Dr. Santiago Camacho-Lopez

The Dissertation of Noe Zamora-Romero is approved:

_____

_____

_____

Committee Chairperson

University of California, Riverside

ACKNOWLEDGEMENTS

I would like to acknowledge my advisor, Dr. Guillermo Aguilar for all his support, and for giving the opportunity to pursue my graduate studies and joining his lab at UCR. Also, my committee members, Dr. Santiago Camacho- Lopez for his advice and encouragement that helped overcome many obstacles during my studies, and Dr. Lorenzo Mangolini, have also being a good source of guidance throughout my graduate studies at UCR.

I want to thank all the colleagues and friends I worked with throughout my graduate studies: Dr Elias Penilla, Dr. Darren Banks, Dr. Kendrick Mensink, Dr Luis F. Devia-Cruz, Dr Alejando Alvarez-Barragan, Ben Sommerkorn and Vicente Robles.

I would like to acknowledge the use of material published in the Journal of Alloys and Compounds, 788 (2019) 666-671. Molybdenum nanoparticles by pulsed laser ablation and effects of oxidation due to aging. N. Zamora-Romero, M. A. Camacho-Lopez, M. Camacho-Lopez, A. R. Vilchis-Nestor, V.H Castrejon-Sanchez, S. Camacho-Lopez, G. Aguilar.

Finally, I need to thank the UC MEXUS-CONACyT Doctoral Fellowship program for providing the financial support for my graduate studies. Additionally, I would also like to thank the Dean's Distinguished Fellowship Award Grant and the UC MEXUS – CICESE Graduate Student Short-Term Research and Non-degree Training grant for the financial support provided.

ABSTRACT OF THE DISSERTATION

Synthesis of Molybdenum Oxide Nanostructures by Using The Laser Ablation of Solids in Liquids Technique

by

Noe Zamora-Romero

Doctor of Philosophy, Graduate Program in Materials Science and Engineering
University of California, Riverside, December 2019
Dr. Guillermo Aguilar, Chairperson

Laser ablation of solids in liquids (LASL) is a straightforward, clean and versatile method that has been used successfully to synthesize nanostructures (NS) with very different sizes, compositions and structures. However, due to the complexity of the laser-matter processes and the technical difficulty to study the phenomena involved, the physical and chemical mechanisms in which NS are generated and evolved in time respectively are not well understood.

On the other hand, one of the oxides that has attracted the attention of several researchers mainly due to its optical and chemical properties is molybdenum oxide (MoO_x). These NS have been synthesized mainly by chemical methods and proposed to be used for several potential applications, from optical and electronic to energy and biological systems since its optical properties can be tuned from the ultraviolet (UV) to near infrared (NIR) range by modifying their size, chemical composition and/or structure.

However, in spite of the recent popularity of MoO_x NS, the LASL method and their potential applications, there are very few studies that report the generation of this type of NS by this method and they lack the explanation of the oxidation process which plays an important part on the optical properties as the first part of this work shows. A picosecond pulsed laser is used for inducing ablation of the Mo target and generate nanoparticles (NPs). Besides, a mechanism of the NPs oxidation process is proposed, and the average diameter and size distribution as function of irradiation energy are discussed.

Furthermore, MoO_x NS have been successfully synthesized by chemical methods and utilized in pothothermal therapy (PTT) in *in vitro* experiments, as PTT agents. This can be possible due to these NS show good biocompability and NIR light absorption, and great phothermal conversion efficiency. Nevertheless, these NS had never been synthesized by the LASL method with the idea of using them as PPT agents with a nanosecond pulsed laser before this work as far as we know.

A Nd:YAG pulsed laser was utilized to generate the core-shell type NPs and the spectroscopy studies show these NS exhibit a peak of absorption in the NIR range, which makes them suitable for PTT. Besides, in order to study the NPs fragmentation phenomena, two irradiation times were used, and a correlation with the average diameter and size distribution was found.

In summary, this research studies how different laser parameters influence the composition of the diverse NS generated, focusing on the effect of intensity, duration of the pulse and time of irradiation when synthesizing molybdenum oxide NS by the LASL method.

Table of Contents

List of Figures

List of Symbols

MoOx	Molybdenum oxide	2
MoO_3	Molibdenum trioxide	2
xH_2O	Water	2
O	Oxygen	2
Nd-YAG	Neodimion Ytria Aluminium Garnet	3
T	Temperature	6
P	Pressure	6
CM	Concentration of the ablated material	6
CS	Concentration of solutions species	6
τ_{pulse}	Pulse duration	8
MoO_5	Molibdenum pentoxide	9
MoO_2	Molibdenum dioxide	9
MoO_6	Molybdate beta	9
ReO_3	Rhenium trioxide	10
UV	Ultra violet	10
NIR	Near infrared	10
L-M	Laser-Mater	11
r_B	Bohr radius	13
τ_e	Elect	13
Te	Electronic temperature	14

Chapter 1

1.1 Introduction

Almost 60 years have passed since the day that Theodore Maiman invented the first laser in his laboratory at Hughes Research Laboratories in Malibu in 1960. Maiman successfully created the first operating laser by using a flash lamp and ruby crystal as optical pump that generated pulsed laser radiation at 694 nm. However, the revolutionary device did not have an application at that time [1]. Nowadays, lasers have been used in a big variety of applications. In materials science, the use of short (nanoseconds) and ultrashort (pico and femtoseconds) pulses for synthesizing different materials, particularly nanostructures (NS) is a very active field of research.

One the most popular and effective methods to fabricate NS by using a laser is the laser ablation of solids in liquids (LASL) technique. In this method, a target which is submerged in a liquid is irradiated with laser pulses that pass through the liquid layer and penetrate into the surface of the material. Because of the interaction between the strong electrical field generated by the laser light and the target surface, the irradiated area is heat up and vaporize, which creates plasma that contains different reactive species such as atoms, molecules and clusters that will nucleate and grow into desirable nanostructures in a cool liquid medium [2, 3].

Pulse length is one the most important parameters in LASL since the physics phenomena behind laser-matter interaction that occurs depends on it, and this affects the features of the NPs generated as it will be discussed in the first part of this work [4-6]. On

the other hand, there are few papers that report the synthesis of molybdenum oxide (MoO_x) NS by using the LASL technique [7-9], and they do not: *i)* explain the oxidation process due to aging and *ii)* explore the synthesis of NS with properties for potential phothermal therapy [10-14].

This is why, the purpose of this work is designing and building a hybrid chemical-physical laser system to study the effects of pulse length and intensity on the generation of NS by using the LASL technique with ps and ns pulsed lasers. The first part of my work explains the generation of NPs composed of molybdenum trioxide hydrated ($MoO_3 \cdot xH_2O$) (x = 1, 2) by using a ps laser and studies the oxidation due to aging [15].

The first set of experiments were made by using an Nd:YAG pulsed laser, which irradiated a highly pure Mo target disk submerged in DI water which forms a 1 cm height column, at room temperature with no especial ambient conditions. The laser repetition rate, and the ablation time were kept constant. The absorption evolution of the obtained colloids was characterized by optical absorption spectroscopy, TEM was used to study the MoO_x NPs morphology, size and structure and Raman spectroscopy to determine the material chemical composition. The second part of my work covers the synthesis of MoO_x nanoparticles (NPs), which exhibit absorption in the biological optical window by using the LASL technique with nanosecond (ns) pulses. PTT is one of the most promising techniques to treat cancer, it has shown remarkable results for selective tumor ablation, some of the advantages of this therapy are that is noninvasive and relatively easy to perform [16-20].

Finding the most suitable PTT agent is essential for the progress and possible implementation of this therapy in clinical trials, nevertheless it has been still a challenge for researchers and scientists because of the peculiar properties this material should have. Moreover, in order to study the effect of fragmentation on the NPs properties, two experiments were carried out. In the first one, the target was ablated for 30 minutes continuously. In the second one, the same target was ablated for 20 minutes, then it was taken out of the container and the colloidal solution generated was irradiated for 10 minutes.

An Nd:YAG laser was used to synthesize the NPs in deionized (DI) water free of surfactants or additives, which were optically characterized by absorption spectroscopy. Semi spherical core-shell NPs were imaged with TEM-EDX and micro-Raman spectroscopy studies determine that the shell of these NPs are composed of amorphous molybdenum oxide hydrates ($MoO_3 \cdot xH_2O$).

References

[1] Alan Chodos, *"*Maiman Builds First Working Laser*", American Physical Society*. Vol. 19, Number 5, May 2010.

[2] J.J Naddeo, D.M. Bubb, "Mechanisms of nanoparticle generation by laser ablation in liquids", *Sprinter Sci. Business media Dordrech*, 2015.

[3] H. Zeng, X.D. Du, S.C. Singh, S.A. Kulinich, S. Yang, J. He, W. Cai, Nanomaterials via Laser Ablation/Irradiation in Liquid: A Review, Adv. Funct. Mater. 22 (2012) 1333–1353.

[4] S. I. Dolgaev , A. V. Simakin , V. V. Voronov , G. A. Shafeev , F. Bozon-Verduraz, "Nanoparticles produced by laser ablation of solids in liquid environment", *Appl. Surf. Sci.* 2002 ,*186* , 546.

[5] V. Amendola, M. Meneghetti, "What controls the composition and the structure of nanomaterials generated by laser ablation in liquid solution?", *Phys.Chem. Chem. Phys.*, 2013, 15, 3027.

[6] J. Dowden, "The theory of laser materials processing", *Springer series in materials science,* 119, heat and mass transfer in modern technology, 2008.

[7] Isabela Alves de Castro, Robi Shankar Datta, Jian Zhen Ou, Andres Castellanos-Gomez, Sharath Sriram, Torben Daeneke, and Kourosh Kalantar-zadeh, "Molybdenum Oxides – From Fundamentals to Functionality" *Adv. Mater.* 2017, 1701619.

[8] Won-Sik K, *et al*., "Gas sensing properties of MoO_3 nanoparticles synthesized by solvothermal method", *Journal of Nanoparticle Research,* Vol 12, Issue 5, pp 1889–1896, June 2010.

[9] Matsuoka Y, Niwa M, Murakami Y., "Morphology of molybdena supported on various oxides and its activity for methanol oxidation", *J Phys Chem* 94:1477, 1990.

[10] J Haber, Lalik HE, "Catalytic properties of MoO_3 revisited", *Elsevier, Catal. Today* 33:119–137, 1997.

[11] Scarminio J, Lourenco A, Gorenstein A, "Electrochromism and photochromism in amorphous molybdenum oxide films", Thin Solid Films 302:66–70, 1997.

[12] M. Mazaa, *et al*., "Valency control in MoO32d nanoparticles generated by pulsed laser liquid solid interaction*", J Nanopart Res*, 14:714 2012.

[13] V. T. Karpukhin, M. M. Malikov, M. V. Protasov, T. I. Borodina, G. E. Val'yano, and O. A. Gololobova, Composition, morphology characteristics, and optical properties of molybdenum oxide nanostructures synthesized by the laser ablation method in liquid, High Temp 55 (2017) 870.

[14] S. Spadaro1, M. Bonsignore, E. Fazio, F. Cimino, A. Speciale, D.Trombetta, F. Barreca, A. Saija, F. Neri, Molybdenum oxide nanocolloids prepared by an external sield-assisted laser ablation in water, EPJ Web of Conferences, 167 (2018) 04009.

[15] N. Zamora-Romero, M. A. Camacho-Lopez, M. Camacho-Lopez, A. R. Vilchis-Nestor, V.H Castrejon-Sanchez, S. Camacho-Lopez, G. Aguilar, Molybdenum nanoparticles by pulsed laser ablation and effects of oxidation due to aging. Journal of Alloys and Compounds 788 (2019) 666-671.

[16] J. Shi, Y. Kuwahara, M. Wen , M. Navlani- García, K. Mori, T. An, H. Yamashita, Room-temperature and aqueous-phase synthesis of plasmonic molybdenum oxide nanoparticles for visible-light-enhanced hydrogen generation, Chem. Asian J. 00 (2016) 0–0.

[17] Y. Yang, Y. Yang, S. Chen, Q. Lu, L. Song, Y. Wei and X. Wang, Atomic-level molybdenum oxide nanorings with full-spectrum absorption and photoresponsive properties, Nature communications, 8 (2017) 1559.

[18] W. Yin, T. Bao, X. Zhang, Q. Gao, J. Yu, X. Dong, L. Yang, Z. Gu, Y. Zhao. Biodegradable MoO_x nanoparticles with efficient near-infrared phtothermal and photodynamic therapy at the second biological window. Nanoscale 10 (2018) 1517.

[19] W. Liu, X. Li, W Li, Q. Zahng, H. Bai, J. Li, G. Xi, Highly stable molybdenum dioxide nanoparticles with strong plasmon resonance are promising in photothermal cancer therapy. Biomaterials 163 (2018) 43-54.

[20] Y. Zhan, Y. Liu, H. Zu, Y. Guo, S. Wu, H. Yang, Z. Liu, B. Lei, J. Zhuang, X. Zhang, D. Huang and C. Hu, Phase-controlled synthesis of molybdenum oxide nanoparticles for surface enhanced Raman scattering and photothermal therapy, Nanoscale, 10(2018)5997-6004.

Chapter 2 Theoretical Background

The laser ablation of solids in liquids (LASL) technique has been used for synthesizing nanostructures (NS) for decades. Recently, nanomaterials with different structures, shapes, physical and chemical properties have been successfully generated by using this method. Noble metal nanoparticles, quantum dots, semiconductor heterostructures, multiphase core-shell oxides among others have been produced [1-3]. The most common products fabricated by the LASL technique are metal NPs or NPs of metal compounds formed due to the reaction of ablated material with liquid media [4]. The main stages of the LASL technique can be summarized as follows (fig. 2.1) [5]:

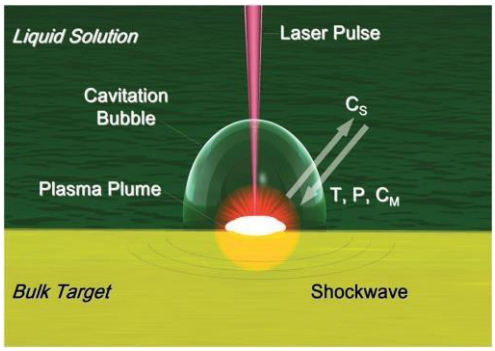

Fig. 2.1. Sketch of the main stages of LASL. The white arrows indicate that, upon increasing the distance from the laser spot, the temperature (T), pressure (P) and concentration of the ablated material (CM) decrease, while the concentration of solution species (CS) increases.

The laser pulse is absorbed by the target, right after a plasma plume containing the ablated material expands into the surrounding liquid, accompanied by the emission of a shockwave. During the expansion, the plasma plume cools down and releases energy to

the liquid solution. This phenomenon generates a cavitation bubble which expands in the liquid and then collapses and emits a second shockwave.

Four parameters whose profiles in time and space predominantly determine the phase and structure of final NPs have been identified: temperature (T), pressure (P), concentration of the ablated material (CM) and concentration of solution species (CS). Due to the hemispherical symmetry of the laser ablation phenomena, the four parameters are not uniform in space neither constant in time. In order to understand better the evolution of these parameters a temporal sequence has been described (fig. 2.2) [5-8].

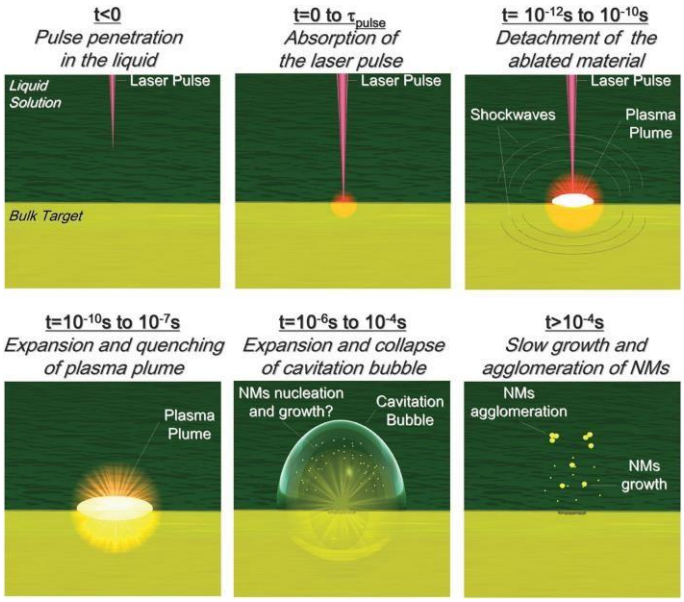

Fig. 2.2. Sketch of the main stages of LASL on time.

For $t < 0$: *pulse penetration in the liquid.* The laser pulse pass through a layer of liquid before reaching the target. With a pulse duration (τ_{pulse}) of ps or longer, breakdown of liquid is avoided by working under defocused conditions. With τ_{pulse} of fs, relevant nonlinear optical effects like self-focusing are observed at fluences required for laser ablation. From $t = 0$ s to τ_{pulse}: *absorption of the laser pulse*. Due to the high photon density, linear and nonlinear absorption processes occur when the laser pulse hits the target. Direct photoionization is highly probable for a pulse duration of up to 10^{-8} s. However, by increasing τ_{pulse} above 10^{-12} s, that is the minimum time required for the electron–lattice thermalization, the electron kinetic energy can be released as thermal energy to the lattice.

For $t = 10^{-12}$ s to 10^{-10} s: *detachment of the ablated material*. Electron–ion collisions initiate, on a timescale of 10^{-12} s, then the detachment of matter from the target happens. When energy is transferred to the target by ps and fs pulses, the ablation mechanism is generically defined as "fragmentation" and consists of the detachment of hot atoms, vapors and liquid drops under out of equilibrium conditions.

For $t = 10^{-10}$ s to 10^{-7} s : *expansion and quenching of plasma plume*. In liquid, target ablation takes place by energy transfer both from the laser pulse to the solid target and from the plasma plume to the heated target.

For $t = 10^{-6}$ s to 10^{-4} s : *expansion and collapse of cavitation bubble*. The energy released by the plasma plume to the surrounding liquid induces the rise of a cavitation bubble, which expands with supersonic speed in the liquid. Bubble's temperature decreases and bubble's internal pressure drops to a value lower than in the surrounding liquid. At this stage, the bubble collapses emitting a shockwave. This is the last physical process related to laser ablation of a target in liquid solution.

For $t > 10^{-4}$ s : *slow growth and agglomeration of NPs*. The system reaches steady state physical and chemical conditions. In this stage, NPs can undergo minimal modifications due to the condensation of ablated atoms and molecular clusters that still survive in solution.

On the other hand, one of the oxides that has attracted the attention of several groups are MoO_x [9-18]. MoO_x have several stochiometries, ranging from full stoichiometric MoO_3, to more conducting reduced oxides in the form of MoO_{3-x} ($2 < x < 3$) and eventually semi-metallc MoO_2 [16]. The two most common crystal phases of MoO_3, are the thermodynamically stable orthorhombic α-phase and metastable monoclinic β-phase both are constructed in different ways, based on the MoO_6 octahedron building block (fig 2.3 a) [19-22].

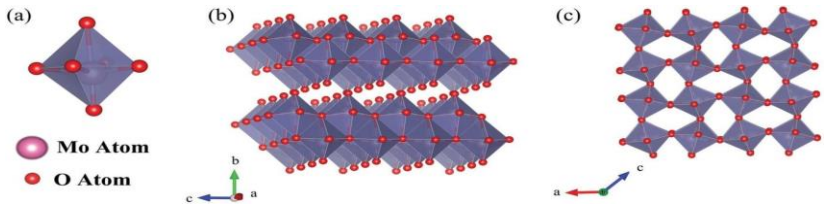

Figure 2.3. a) MoO_6 octahedra as found in the thermodynamically stable α-MoO3 composed of molybdenum and oxygen atoms. b) Thermodynamically stable orthorhombic α-MoO3 with layered structure held together by van der Waals' forces. c) Metastable monoclinic β-MoO3.

Orthorhombic α-MoO3 (fig. 2.3 b), possesses a layered crystal structure of MoO_3 which offers the possibility to create two dimensional morphologies. The crystal structure of β-MoO_3 (fig. 2.3 c) is similar to ReO_3 in which the MoO_6 octahedra share corners in three dimensions establishing a monoclinic structure. It has been reported that a transition from β-MoO3 to α-MoO3 occurs as a result of thermal treatments at temperatures above 350 °C [20].

In the case of monoclinic MoO_2, it displays a deformed rutile structure as shown in figure 5. The rutile structure represents a tetragonal orientation, where the MoO_6 octahedra chains share opposite edges along the crystallographic *c*-axis [22-23].

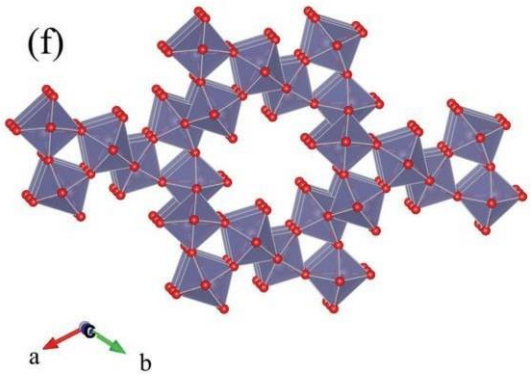

Figure 2.4. MoO_2 structure, it shows a tunnel structure along the c-axis of h- MoO_3 unit cell.

Different MoO_x NS have been synthesized and proposed to be used in a wide range of potential applications, from optical and electronic to energy and biological systems, this can be possible since its optical properties can be tuned from the ultraviolet (UV) to near infrared (NIR) range by modifying their size, chemical composition and/or structure [21].

2.1 Laser-Matter Interactions

To describe the laser and matter (L-M) interaction, in which only a small number of physical phenomena contribute, four parameters can be selected, namely photon energy, laser intensity, pulse duration and beam radius. Even though there are indications of the existence of different physical domains in L- M interactions which can be classified only by pulse duration (fig 2.5) and intensity (fig. 2.6) [24].

2.2 Pulse duration

One of the critical parameters in laser ablation is pulse duration (τ_{pulse}), due to it has a strong influence on NPs size distribution, structure and composition [25]. By using the same fluence but increasing τ_{pulse}, thermal mechanisms of ablation are favored at the expense of photoionization mechanisms. [25-30].

When using fs pulses, ablation is dominated by direct photoionization processes. With pulses of tens of ps or longer the coexistence of direct photoionization and thermal ablation processes like vaporization, boiling and ejection of melted material occur [26]. With ns pulses, the ablated material and the laser pulse coexist for a relatively long time due to plasma shielding, part of the energy is transferred to the plasma plume which increases its temperature, pressure and lifetime [31, 32].

There exist three physical domains distinguished by the corresponding time scales namely, cold ablation, hot ablation and melt expulsion as seen in figure 2.5 [33].

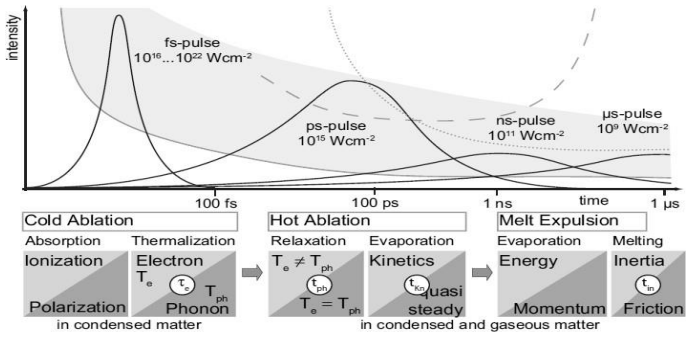

Fig. 2.5. Mapping of the three different physical domains – Cold Ablation, Hot Ablation and Melt Expulsion – with respect to the corresponding time scales.

The ablation threshold (solid line), the maximum available pulse energy (grey) and the threshold for the critical state (dashed) of matter are indicated qualitatively. For long pulse durations the radiation also interacts with the ablated material in the gaseous phase (plasma threshold, dotted line). Typical time scales for thermalization of electrons τ_e, relaxation of phonon temperature τ_{ph}, for kinetics in the Knudsen layer approaching a quasi-steady state t_{Kn} and the onset of fully developed melt flow tin limited by inertia are given.

2.3 Cold ablation

In cold ablation, thermalization of the photon energy absorbed by the electrons leads to a thermodynamic equilibrium in the electron system, which establishes an electron temperature. This happens for τ_{pulse} smaller than $t_p < 100$ fs, absorption of radiation initiates and after a few ps, the phonon temperature rises and ablation of hot matter starts to take place.

Metals have a large electron density and a pulse duration of some femtoseconds is long time compared with the atomic scale r_B/ v_e. With $r_B= 5.3x10^{-11}$ m, the Bohr orbit, and the electron velocity $v_e= 2.2X10^6$ m/s [34]. Thus, absorption and subsequent cold ablation can happen without thermalization of energy.

Thermalization of electrons by electron-electron collisions at $\tau_e \sim 10$ ps is much faster than the thermalization of electrons of phonons. The time scale τ_e for relaxation of energy in the electron system can be related to the final temperatures T_e and T_{ph} which the subsystems of electrons and phonons approaching thermalization as follows [35]:

$\tau_e = (\tau_{e-e}^{-1} - \tau_{e-ph}^{-1})^{-1} = (A\, T_e^2 +$

The constants A and B are related to electron-electron and electron-phonon collision frequencies of the material.

During beam-matter interaction for a fs [36] and ps-pulse [37], matter passes through one of at least four different possible paths in the physical phase space as seen in figure 9, this has been calculated by molecular dynamics.

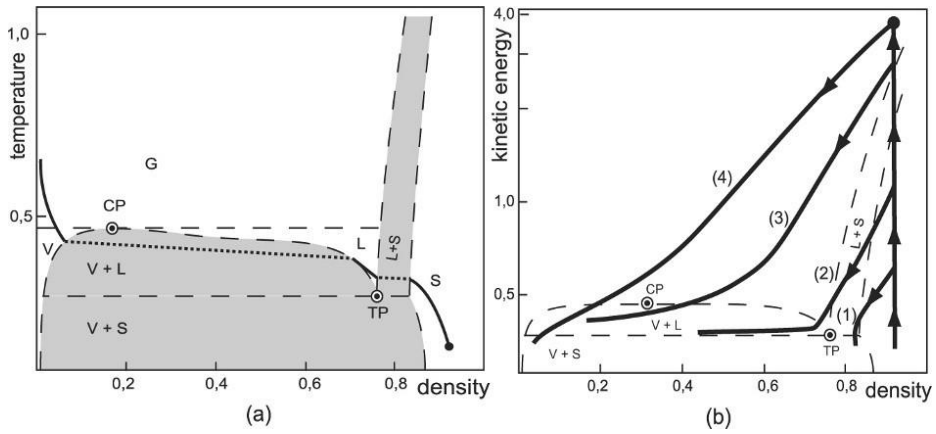

Fig. 2.6 (a) A typical path in the phase space for pulses longer than tp _ 100 ps is related to the processing domain called "Melt Expulsion". Abbreviations are G Gaseous, V Vapor, L Liquid, S Solid, TP Triple Point, CP Critical Point. (b) The physical path in the phase space of a pre-selected material volume related to the action of a fs-pulse. The physical path is projected onto a sub-space spanned by kinetic energy instead of temperature and density. For reference, the binodal lines of the state of matter diagram for thermodynamical equilibrium are indicated (dashed). Depending on the energy absorbed, the dynamics of the matter volume follows four different paths in the physical phase space indicated by (1) spallation, (2) nucleation, (3) fragmentation and (4) vaporization.

Molecular dynamics calculations show that the pulse energy is a dominant parameter for the selection of the path in a phase space. On the right of the diagram near the ablation threshold, we can see spallation (1), no gaseous phase is involved, while the thermo-mechanical load exceeds the yield stress of the material and removal like spalling of a thin metal disk is observed. The nucleation (2) path goes through the liquid phase as well as through the coexistence of a liquid-solid phase, and ends in the coexistence of a liquid-gas phase.

Employing a phenomenological interpretation, nucleation is characterized by the development of vapor bubbles in homogeneously boiling molten material. For the last two ablation mechanisms, fragmentation (3) and vaporization (4), ablation occurs outside the liquid-solid and liquid vapor-coexistence regions, having the effect that the mass is separated from the surface just before relaxation to thermodynamic equilibrium becomes noticeable. The two paths are differentiated by cluster formation, which takes place in fragmentation (3) and is absent in vaporization (4).

2.4 Hot ablation

In hot ablation, the radiation interacts with both condensed and gaseous matter for τ_{pulse} around t_p = 100 ps. Electron and phonon temperatures are well defined thermodynamically parameters and phonons as well as the formation of a dissipative heat flux are the main physical effects encountered [38].

Generally the initial heat flux Q_e if the electrons is much smaller than the spatial change $Q_e << -\lambda_e \Delta U_e / C_e \propto \Delta T_e$ of the energy U_e absorbed by the electrons. A detailed discussion of the dynamics involved by analyzing the hyperbolic two- temperature model is given in [39].

$$\frac{\partial U_e}{\partial t} + \frac{Q_e}{\partial z} = I_0 \, A_0 \, f(t) \, \alpha \, e^{-\alpha z} + h_{ex}(T_{ph} + T_e) \tag{1}$$

$$\tau_{Q_e} \frac{\partial Q_e}{\partial t} + Q_e = - \lambda_e \frac{\partial T_e}{\partial z} \tag{2}$$

$$\frac{\partial U_{ph}}{\partial t} + \frac{\partial Q_{ph}}{\partial z} = h_{ex} \, (T_e - T_{ph}) \tag{3}$$

$$\tau_{Q_{ph}} \frac{\partial Q_{ph}}{\partial z} + Q_{ph} = - \lambda_{ph} \frac{\partial T_{ph}}{\partial z} \tag{4}$$

Here the absorption of the laser radiation is described by the term $_0 \; A_0 \; f(t) \alpha \, e^{-\alpha z}$, where $I_0 \; f(t)$ is the time-dependent intensity of the radiation $A_0 = 1 - R0$, is the degree of transmission at the surface related to the degree of reflection R 0, and α^{-1} is the penetration depth of the laser radiation. The thermal diffusivity of the phonons can be neglected compared to the electron diffusivity, $\lambda_{ph} / C_{ph} << \lambda_e / C_e$.

Time scale separation for relaxation in the electron and phonon systems is pronounced. The long time limit for the heat flux Q_e of the electrons, which is given by Fourier's Law $Q_e = -\lambda_e \nabla U_e / C_e$, is established during the same very short time $\tau_{Qe} \sim \tau_e \sim$ 10fs that the thermalisation of the electron system requires [35, 39]. For pulse durations much longer than τ_{Qe} the relaxation of the heat flow is negligible, thus showing that the standard parabolic two-temperature model of Anisimov is adequate, where the idealized assumption of instantaneous heat propagation is assumed [33].

2.5 Melt expulsion

In the case of melt expulsion, evaporation takes a dominant role in the absorption of energy for ns pulses, but only a small amount of momentum is transferred to the melt, and melt ejection sets in [40]. For τ_{pulse} greater than 100 ps the energy is dissipated in local thermal equilibrium. Thermal emission of electrons from condensed matter and collisional effect dominate the formation of ionized vapor or plasma [41].

2.6 Radiation intensity

The intensity of the radiation induces different types of beam-matter interaction in metals since ionization and excitation processes depend on both photon energy and the number density of photons. At least four domains can be differentiated with respect to intensity, which are characterized by heating of matter, the effects of sub- and super-atomic field strengths as well as the properties of relativistic particles (**Fig. 2.7**).

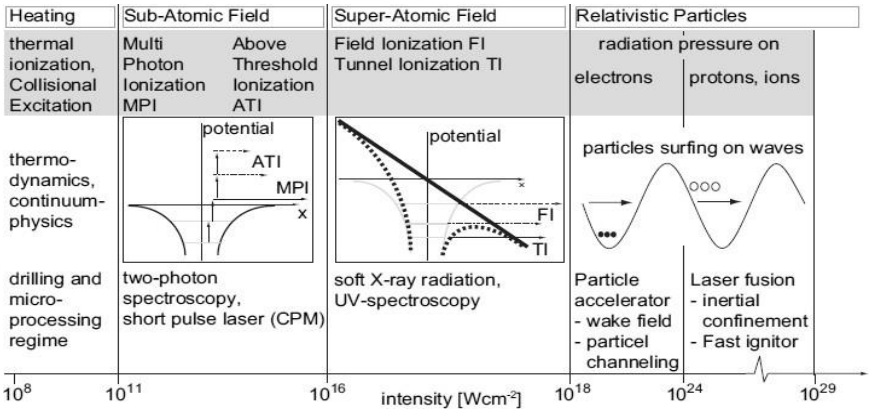

Fig. 2.7 Mapping of the different physical domains – Heating, Sub- and Super- Atomic Field Strength as well as Relativistic Particles – with respect to the corresponding intensity for metals.

At intensities lower than 10^{11} W/cm^2 absorption of infrared radiation in metals basically behaves optically linearly and elevated temperatures are established via Joule heating of the atoms by collisions with excited electrons from the conduction band. At higher intensities above 10^{11} W/cm^2 multi-photon absorption or multi-photon ionization (MPI) in the infrared spectrum are observable [42].

Above-threshold ionization (ATI) is a kind of beam-matter interaction in which atoms subject to intense laser fields at intensities above 10^{12} W/cm^2 absorb more than the minimum number of photons required for ionization. Field ionization (FI) and tunnel ionization (TI) come into play at intensities where the laser field E changes the atomic structure by ponderomotive forces. At intensities above $I > 10^{16}$ W/cm^2 the electrical field strength becomes comparable with typical atomic fields.

At 10^{18}–10^{19} W/cm^2 the travel distance an electron needs to pick up its own rest energy $m_e c^2$ is only one wavelength λ of the incident visible light $eE\lambda = m_e c^2$ and the motion of

the electron becomes relativistic. The energy of the wave becomes so large that the electron "surfs" on the wave. The wave exerts direct light pressure on the electron. The plasma and the particles become relativistic, the mechanisms lead to concepts and realization for particle acceleration and to free electron lasers.

At intensities I =10^{24} W/cm^2, the same effect occurs not only for electrons - they ontinue surfing at the bottom of this wave - but also for heavy protons with mass mp. The proton motion becomes relativistic $eE\lambda = mpc^2$.

The LASL method differs from laser ablation in vacuum or gaseous environments since the liquid can help to control some of the parameters of fabrication and to obtain the desired morphology and microstructure [43]. This technique is promising since the NPs formed can be free of both surfactants and other ions that exist during chemical synthesis [44].

My doctoral work encompasses studies in effects of pulse length from femto and pico to nanoseconds on the ablation process and the variation of the optical, chemical and structural properties of the NS formed for a variety of experimental conditions, focusing on the effect of both intensity and duration of the pulse when synthesizing molybdenum oxide nanoparticles by the LASL method.

References

[1] P. Liu, H. Cui, C. X. Wang and G. W. Yang, "From nanocrystal synthesis to functional nanostructure fabrication: laser ablation in liquid", Phys. Chem. Chem. Phys., 2010, 12, 3942–3952.

[2] H. Zeng, X.D. Du, S.C. Singh, S.A. Kulinich, S. Yang, J. He, W. Cai, Nanomaterials via Laser Ablation/Irradiation in Liquid: A Review, Adv. Funct. Mater. 22 (2012) 1333–1353.

[3] S. I. Dolgaev , A. V. Simakin , V. V. Voronov , G. A. Shafeev , F. Bozon-Verduraz, "Nanoparticles produced by laser ablation of solids in liquid environment", *Appl. Surf. Sci.* 2002 ,*186* , 546.

[4] E. V. Barmina, G. A. Shafeev, P. G. Kuzmin, A. A. Serkov, A. V. Simakin, N. N. Melnik, "Laser-assisted generation of gold nanoparticles and nanostructures in liquid and their plasmonic luminescence", *Appl. Phys*. A (2014) 115:747–752.

[5] Stefano Scaramuzza, Mirco Zerbetto, and Vincenzo Amendola, "synthesis of gold nanoparticles in liquid environment by laser ablation with geometrically confined configurations: insights to improve size control and productivity", *J. Phys. Chem*. C 2016, 120, 9453−9463.

[6] Fumitaka Mafune´, Jun-ya Kohno, Yoshihiro Takeda, and Tamotsu Kondow, Hisahiro Sawabe, "Formation of Gold Nanoparticles by Laser Ablation in Aqueous Solution of Surfactant", *J. Phys. Chem*. B 2001, 105, 5114-5120.

[7] S Dolgaev, *et al*., "Nanoparticles produced by laser ablation of solids in liquid enviroment", *Appl surface Sci*., 186, 2002, 546-551.

[8] Takeshi Sasaki, Yoshiki Shimizu, Naoto Koshizaki, "Preparation of metal oxide-based nanomaterials using nanosecond pulsed laser ablation in liquids", *Journal of Photochemistry and Photobiology A*: Chemistry 182 (2006) 335–341.

[9] Haibo Zeng, Weiping Cai,* Yue Li, Jinlian Hu, and Peisheng Liu, "Composition/Structural Evolution and Optical Properties of ZnO/Zn Nanoparticles by Laser Ablation in Liquid Media", *J. Phys. Chem. B* 2005, *109,* 18260-18266.

[10] I. Rocha-Mendoza, S. Camacho-López, Y. Luna-Palacios, Y. Esqueda-Barrón, M. A. Camacho-López, M. Camacho-López, G. Aguilar, "Second- harmonic generation of ZnO nanoparticles synthesized by laser ablation of solids in liquids", *Optics and Laser Technology*, 99 (2018) 118–123.

[11] M.A. Gondala, Tawfik A. Salehb, Q.A. Drmosh, "Synthesis of nickel oxide nanoparticles using pulsed laser ablation in liquids and their optical characterization", *Applied Surface Science* 258 (2012) 6982– 6986.

[12] Csaba La´szlo´ Sajti,† Ramin Sattari, Boris N. Chichkov, and Stephan Barcikowski, "Gram Scale Synthesis of Pure Ceramic Nanoparticles by Laser Ablation in Liquid", *J. Phys. Chem. C* 2010, 114, 2421–2427.

[13] Yu-Hung Chen, Chen-Sheng Yeh, "Laser ablation method: use of surfactants to form the dispersed Ag nanoparticles", *Colloids and Surfaces A: Physicochemical and Engineering Aspects* 197 (2002) 133–139.

[14] I.A. Sukhov, G.A. Shafeev, V.V. Voronov, M. Sygletoub, E. Stratakis, C. Fotakis, "Generation of nanoparticles of bronze and brass by laser ablation inliquid", *Applied Surface Science* 302 (2014) 79–82.

[15] D. Reyes-Contreras, M. Camacho-López, M. A. Camacho-López, S. Camacho-López, R. Rodríguez-Beltrán, M. Mayorga-Rojas, "Influence of the per pulse laser fluence on the optical properties of carbon nanoparticles synthesized by laser ablation of solids in liquids". *Optics & Laser Technology* 74 (2015) 48–52.

[16] Yi-Pei Lee, Yi-Hsin Liu and Chen-Sheng Yeh, "Formation of bayerite, gibbsite and boehmite particles by laser ablation", *Phys. Chem. Chem. Phys*., 1999, 1, 4681È4686.

[17] Emmanuel Stratakis, Marios Barberoglou, Costas Fotakis, Guillaume Viau, Cecile Garcia, and Georgy A. Shafeev, "Generation of Al nanoparticles via ablation of bulk Al in liquids with short laser pulses", 2009 / Vol. 17, No. 15 / *Optics express* 12650.

[18] E.B. Barmina, E. Stratakis, C. Fotakis, G.A. Shafeev, "Generation of nanostructures on metals by laser ablation in liquids: new results", *Quantum Electronics* 40 (11) 1012 ë 1020 (2010).

[19] M. Camacho-López, M. A. Camacho-López, D. Reyes-Contreras, A. Arrieta-Castañeda, R. Vilchis-Nestor, S. Camacho-López, "Synthesis of CdTe quantum dots by means of laser ablation MACL". *Superficies y Vacío* 27(3) 93-97, 2014.

[20] S. Dadashi, R. Poursalehi, H. Delavari, "Optical and structural properties of Bi-based nanoparticles prepared via pulsed Nd:YAG laser ablation in organic liquids", *Applied Physics A* (2018) 124:406.

[21] S. Dadashi, R. Poursalehi, H. Delavari H, "Formation, gradual oxidation mechanism and tunable optical properties of Bi/Bi2O3 nanoparticles prepared by Nd:YAG laser ablation in liquid: Dissolved oxygen as genesis of tractable oxidation", Materials Research Bulletin 97 (2018) 421–427.

[22] J.J Naddeo, D.M. Bubb, "Mechanisms of nanoparticle generation by laser ablation in liquids", *Sprinter Sci. Business media Dordrech*, 2015.

[23] M. Hashida , H. Mishima , S. Tokita , S. Sakabe, "Non-thermal ablation of expanded polytetrafluoroethylene with an intense femtosecond-pulse laser", *Opt. Express* 2009 , *17* , 13116.

[24] J. Dowden, "The theory of laser materials processing", *Springer series in materials science,* 119, heat and mass transfer in modern technology, 2008.

[25] V. Amendola, M. Meneghetti, "What controls the composition and the structure of nanomaterials generated by laser ablation in liquid solution?", *Phys.Chem. Chem. Phys.,* 2013, 15, 3027.

[26] L. V. Zhigilei, Z. Lin and D. S. Ivanov, "Atomistic Modeling of Short Pulse Laser Ablation of Metals: Connections between Melting, Spallation, and Phase Explosion", *J. Phys. Chem. C*, 2009, 113, 11892–11906.

[27] D. Perez and L. J. Lewis, "Molecular-dynamics study of ablation of solids under femtosecond laser pulses", *Phys. Rev. B: Condens. Matter, Mater. Phys*., 2003, 67, 184102.

[28] D. Perez, L. K. Be´land, D. Deryng, L. J. Lewis and M. Meunier, "Numerical study of the thermal ablation of wet solids by ultrashort laser pulses", *Phys. Rev. B: Condens. Matter Mater. Phys*., 2008, 77, 014108.

[29] P. Lorazo, L. J. Lewis and M. Meunier, "Short-Pulse Laser Ablation of Solids: From Phase Explosion to Fragmentation", *Phys. Rev. Lett*., 2003, 91, 225502.

[30] P. Lorazo, L. J. Lewis and M. Meunier, "Thermodynamic pathways to melting, ablation, and solidification in absorbing solids under pulsed laser irradiation", *Phys. Rev. B*: Condens. Matter Mater. Phys., 2006, 73, 134108.

[31] C. Momma, B. N. Chichkov, S. Nolte, F. von Alvensleben, A. Tu¨nnermann, H. Welling and B. Wellegehausen, "Short-pulse laser ablation of solid targets", *Opt. Commun*., 1996, 129, 134–142.

[32] J. H. Yoo, S. H. Jeong, X. L. Mao, R. Greif and R. E. Russo, "Evidence for phase-explosion and generation of large particles during high power nanosecond laser ablation of silicon", *Appl. Phys. Lett*., 2000, 76, 783–785.

[33] Kostrykin V, Niessen M, Jandeleit J, Schulz W, Kreutz EW, Poprawe R, "Picosecond laser pulses induced heat and mass transfer. In: High-Power Laser Ablation", Santa Fe, Phipps CR (ed), *SPIE Proceedings* vol 3343: 971– 982, 1998.

[34] Brabec T, Krausz F, "Intense few-cycle laser fields: Frontiers of nonlinear optics". *Rev Mod Phys*, 72: 545, 2000.

[35] Wang X, Riffe D, Lee Y, Downer M, "Time resolved electron temperature measurement in highly excited gold target using femtosecond thermionic emission". *Phys Rev B* 50: 8016–8019, 1994.

[36] Perez D, Lewis LJ, "Molecular dynamics studies of ablation of solids under femtosecond pulses*". Phys Rev* B67: 184102, 2003.

[37] Zhigilei LV, Garrison BJ, "Microscopic mechanisms of laser ablation of organic solids in thermal and stress confinement irradiatin regimes". *J Appl Phys* 88(3): 1281–1298, 2000.

[38] Wang X, Riffe D, Lee Y, Downer M, "Time resolved electron temperature measurement in highly excited gold target using femtosecond thermionic emission". *Phys Rev B* 50: 8016–8019, 1994.

[39] Kostrykin V, Niessen M, Jandeleit J, Schulz W, Kreutz EW, Poprawe R, "Picosecond laser pulses induced heat and mass transfer". In: High-Power Laser Ablation, Santa Fe, Phipps CR (ed), *SPIE Proceedings* vol 3343: 971– 982, 1998.

[40] Brabec T, Krausz F, "Intense few-cycle laser fields: Frontiers of nonlinear optics", *Rev Mod Phys* 72: 545, 2000.

[41] Yi-Pei Lee, Yi-Hsin Liu and Chen-Sheng Yeh, "Formation of bayerite, gibbsite and boehmite particles by laser ablation", *Phys. Chem. Chem. Phys*., 1999, 1, 4681È4686.

[42] Chin SL, Lambropoulos P, M, "Multiphoton Ionization of Atoms". 1984.

[43] S. I. Dolgaev , A. V. Simakin , V. V. Voronov , G. A. Shafeev , F. Bozon-Verduraz, "Nanoparticles produced by laser ablation of solids in liquid environment", *Appl. Surf. Sci.* 2002, 186, 546.

[44] A. V. Simakin, V. V. Voronov, and G. A. Shafeev, “Nanoparticle formation during laser ablation of solids in liquids”, *Phys. of wave phenomena*. Vol 15, No. 4, pp. 218-240, (2007).

Chapter 3 Molybdenum nanoparticles generation by picosecond pulse laser ablation and effects of oxidation due to aging

Several groups of researchers have investigated the synthesis of different NS composed of metal oxides byusing the LASL method, some of the most important findings will be discuss later in this chapter. However, in the case of MoO_x NS the few reports that exist did not investigate systematically the oxidation process due to aging nor discuss the possible mechanism, and this was part of the motivation for this chapter, which focuses on the synthesis of molybdenum oxide nanoparticles by using picosecond pulses and their oxidation process.

The so-called LASL technique is an effective method to obtain nanostructures [1]. This method is promising since the NPs formed can be free of both surfactants and other ions that exist during chemical synthesis [2], and it differs from laser ablation in vacuum or gaseous environments since the liquid can help to control some of the parameters of fabrication and to obtain the desired morphology and microstructure [3]. In the LASL process, material is removed from the surface of a target in the form of plasma by the application of a high pulsed laser beam. Usually a target is submerged in a liquid and the laser is focused on the target through the transparent medium [4, 5].

When using the LASL method with metals, there are two main formation mechanisms proposed for the generation of nanostructures: i) the thermal evaporation with liquid interaction, and ii) the explosive ejection of nanodroplets. In the former, the formation of nanostructures is associated with the combination of ultrafast quenching of

hot plasma and its interaction with surrounding media [6]. In the latter case, it is suggested that the laser irradiation could cause a local melting from the metal target, the adjacent liquid layer is heated to vapor or plasma state with a high pressure, which splashes the molten target into nanodroplets that react with the liquid medium and create the final nanostructures [7].

Some of the articles that have reported the formation of metal oxides by the LASL method were performed by Dadashi, *et al*., who generated Bi, $Bi(OH)_3$ and α-β-Bi_2O_3 by irradiating with a ns laser a Bi target in DI water. They claimed oxidation happens mainly during ablation, and after ablation slow oxidation and hydroxylation began at the surface of NP forming a shell. As a result, the absorbance peak increased in the 200 to 420 nm range, and after 21 days after the synthesis the NPs suffer from full oxidation [8].

In the same way Rocha-Mendoza, *et al*., synthesized ZnO NPs by irradiating a zinc target in acetone with a ns pulsed laser at 1,064 nm and showed that after synthesis a small ZnO shell starts forming around a Zn core until full oxidation happens after 30 days [9]. In contrast, Lee *et al*., obtained different shapes of NS made of $Al(OH)_3$, ALOOH by irradiating an Al target submerged in either water or distilled water with a ns pulsed laser at 532 nm. Triangular, rectangular and fiber NS made of boehmite, gibbsite, and bayerite were formed, respectively. They claimed NPs absorption decreased for 6 days after irradiation, then started increasing 20 days later and even reached the same value than the first day. However, their reported that NPs formation process was still ambiguous [10].

In the case of MoO_x, despite of all their potential applications, especially in optical and electronic systems and even as photothermal (PTT) agents -this will be covered in the next chapter- [11-21], we have only found three studies so far which include the generation of NPs by using the LASL method, but they lack the explanation of the oxidation process [22-24].

In one study [22], binary oxides nanoparticles were synthesized by using the LASL method, using water or hydrogen peroxide-based coating liquid. Yellow MoO_3 and dark blue hydrated molybdic pentoxide ($Mo_2O_5.xH_2O$) nano- suspensions were obtained by irradiating with a Nd:YAG laser (1064 nm, 95 mJ per pulse) a Mo target. The average size of the MoO_3 NPs was about 8 nm, slightly larger than the $Mo_2O_5 \cdot xH_2O$ at 6.2 nm.

Another study [23] reported the generation of MoO_x NPs with average size of 100 nm by using a 20 ns laser at 510.6 and 578.2 nm with 9–10 W for 3 hrs at 10-12 kHz. The analysis of the structure and the composition of the colloid suspensions with an X-ray diffractometer shows evidence of MoO_3, MoO_2 and Mo NPs. Finally, in [24], oblong and spherical MoO_x NS sizes 20-100 nm were obtained by using an external field-assisted ps laser at 532 nm, 100 kHz for 30 min. Evidence of α-MoO_3 was shown and they observed that there is no cell toxicity when using MoO_x NPs that were synthesized in DI water and ambient conditions.

However, there are several unanswered questions concerning the formation of the MoO_x NPs, especially the ones related to the post laser exposure aging process. For instance, the three studies fail to report either the time in which the spectroscopy studies were carried out or when the TEM micrographs were taken with respect to the date of NPs

synthesis, which clearly plays an important role on the oxide formation or evolution.

The objective of this chapter is to discuss the experiments performed to synthesize NPs composed of molybdenum oxide by using the LASL method and study the oxidation due to aging. A picosecond Nd:YAG laser was used and the per pulse laser fluence was varied. The absorption evolution of the obtained colloids was characterized by optical absorption spectroscopy, TEM was used to study the MoO_x NPs morphology, size and structure and micro-Raman spectroscopy to determine the material chemical composition.

3.1 Experimental

3.1.1 Synthesis of the Mo NPs colloidal suspensions

We used a ps Nd:YAG (Ekspla, Lithuania) pulsed laser to irradiate a highly pure (99.95 %) Mo target disk (*Kurt J, Lesker Co*) submerged in DI water which forms a 1 cm height column, at room temperature with no especial ambient conditions. The laser repetition rate, and the ablation time were kept constant. The laser beam was focused by using a convex lens (**fig. 3.1**) of 200 mm focal length.

The Mo target was rotating while irradiating in order to avoid irradiation on the same target spot. The laser wavelength was at the fundamental 1064 nm, the pulse duration 30 ps, at a 10 Hz repetition rate, and per pulse laser fluence of 5, 10, 15 and 20 J/cm^2 for an exposure time of 5 minutes.

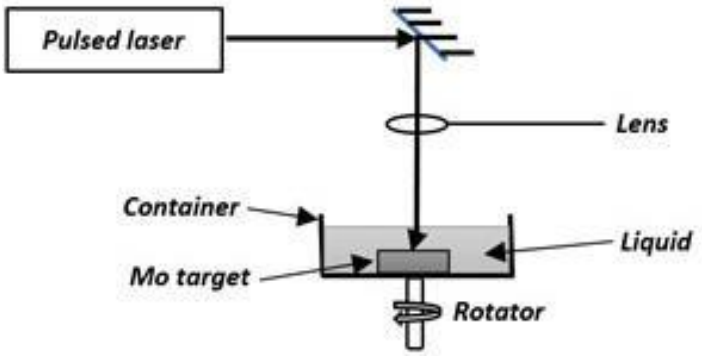

Fig 3.1. LASL experimental set up. Picosecond laser pulses were used to ablate a Mo target submerged in DI water.

3.2 Sample Characterization

3.2.1 UV-Vis Characterization

The optical characterization of the obtained colloidal suspensions was performed using a double beam spectrometer (Lambda 650 Perkin-Elmer) in the 200 to 900 nm range. For this purpose a quartz cuvette with an optical path length of 10 mm was used. The optical absorption spectra were taken on a regular basis right after the NPs synthesis and then for several weeks. All the experiments were ‘performed under normal ambient conditions.

3.2.2 Transmission Electron Microscopy

TEM studies were carried out using a JEOL 2100 microscope operating at 120 kV accelerating voltage with a LaB_6 filament. The samples were prepared by placing drops of the NPs suspension over carbon-coated Cu grids, it was allow to evaporate, then observed in the TEM. In order to obtain information of the particle size, the length of many particles were measured employing ImageJ™ software. Particle size diameters were calculated with the equation $d_{avg} = \Sigma (n_i d_i) / \Sigma n_i$, where n_i is the number of particles of diameter d_i.

3.2.3 Raman Spectroscopy

Raman spectroscopy was used to determine the crystalline structure of MoO_x NPs. Raman spectra were recorded using a micro-Raman Horiba Jobin Yvon system, model Xplora plus. A Solid-state laser (λ=532 nm) was used to induce scattering with a nominal power of 25 mW. The laser beam was focused using a 100x lens and also it serves to recollect scattered light. The laser power on sample's surface was 1% of nominal power. A 1200 lines/mm grating was employed, 100 acquisitions were averaged with an exposure time of 1 s each one.

3.3 Results and discussion

3.3.1 Absorption spectrum of Mo NPs

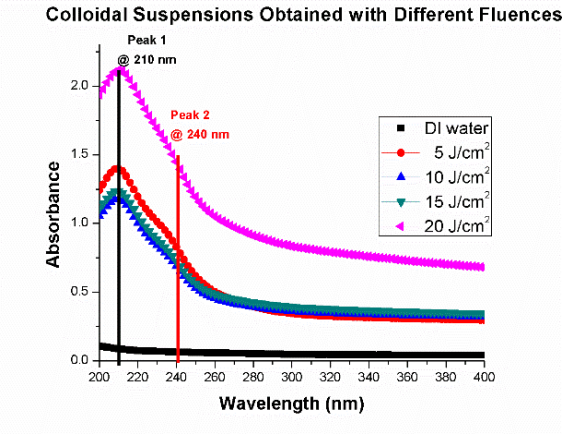

Fig 3.2. MoO_x colloidal suspensions absorbance just after irradiation.

Figure 3.2 shows the absorbance of colloidal suspensions in DI water obtained right after irradiation with different energy fluences from 5 to 20 J/cm^2. The absorbance of DI water is also shown (black squares) as reference. We expected the value of the absorbance to be increased as the irradiation fluence was augmented due to fact that the absorbance is function of NPs concentration and size, and also the generation of larger NPs when irradiating with higher fluences [25]. It can be seen that the absorbance values obtained for 10 (blue upward triangles), 15 (green downward triangles) and 20 J/cm^2 (pink sideward triangles) behave as predicted, but is not the case for 5 J/cm^2 (red circles), since its value is higher than ones obtained for fluences of 10 and 15 J/cm^2. This occurs because the colloidal suspension obtained is more concentrated than the ones obtained with 10 and 15 J/cm^2.

Additionally, the absorbance spectra show a well-defined peak and a shoulder, which can clearly be seen in figure 2, at around 210 nm, and 240 nm, respectively. This is the characteristic absorbance spectrum for spherical Mo NPs [26]. Noble and transition plasmonic metal NPs show similar absorbance spectra [27, 28]. Different sizes of MoO_x NPs have been synthesized by using different synthesis methods that exhibit surface plasmonic resonance peaks in different spectral regions from UV to NIR, [29-31].

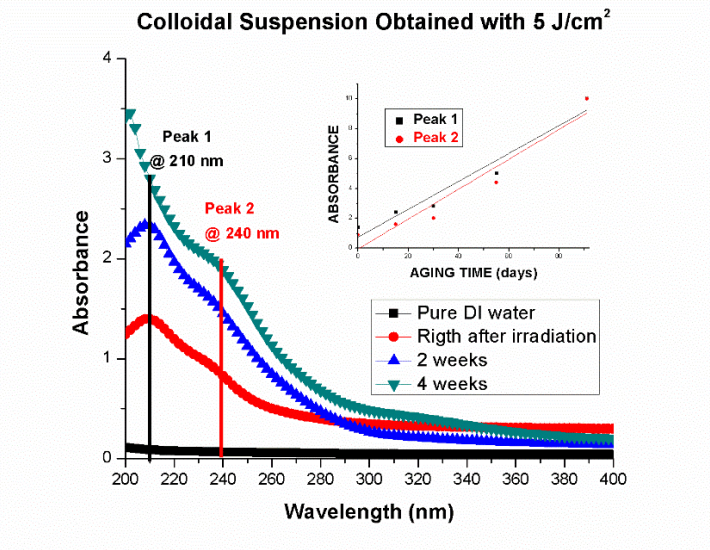

Fig 3.3 MoO_x colloidal suspension absorbance evolution at different times.

Figure 3.3 shows a typical absorbance spectra time evolution of an aging colloidal suspension, which was obtained when irradiating the target with per pulse laser fluence of 5 J/cm^2. It shows that the absorbance increases as the colloidal suspension ages. Right after the ablation of the target, spherical Mo NPs are formed (red circles) according to its absorbance spectrum, which is known in the literature for such kind of Mo NPs with mean

diameter tens of nm [26]. Once in the colloidal suspension, the Mo NPs interact with the surrounding water molecules of the liquid media, which starts surface oxidation of the NPs.

This changes not only the metallic nature of the NPs but also its size and possibly its shape, getting as a result absorbance changes in time. At the end of the second week of aging the absorbance spectrum still shows its peak (vertical black line) at the same position, it is around 210 nm, the same applies for the shoulder (vertical red line) which remains at the 240 nm position, but a subtle shoulder appears around 320 nm.

At 4 weeks aging (green downward triangles) the NPs in the colloidal suspension are more oxidized and remarkably the peak in the absorbance spectrum shifts to shorter wavelength at around 200 nm, while the shoulders at 240 nm and 330 nm are enhanced; this spectrum shows features belonging to characteristic spherical MoO_3 NPs [26]. The inset shows the absorbance values for the peak and the shoulder as the colloidal suspension evolves in time. There is a linear increment of the absorbance as the suspension ages. We believe this can be explained by a growing layer of oxide around the Mo NP, giving place to the formation of a core-shell type structure [32].

3.3.2 TEM images of the MoO_x NPs

Figure 3.4 shows typical images of the different types of NPs found three weeks after irradiation by using a TEM microscopy. As can be seen three types of nanoparticles are present: Mo NPs and MoOx (a), Mo@MoOx (b) and a Mo- MoOx particle. The core of the nanoparticle appears darker because it is denser than the oxide layer that covers the Mo core, around the core the oxide shell has a light grey appearance. 4a) shows a large

spherical Mo NP with a diameter in the order of 199 nm surrounded by a tiny MoO_x layer. Two small MoO_x NPs, are attached, one to the upper right and a second one at the bottom of the Mo NP, with diameters of 65 and 67 nm, respectively. In 4b) a medium size Mo NP can be seen with a diameter of 158 nm and a layer of MoO_x forming a MoO_x@Mo core-shell type of structure.

Finally, in 4c) there is quasi-spherical NP that seems to be formed by an agglomerate of several small nanoparticles, its diameter is around 135 nm and it has the thickest layer of MoO_x out of the three NPs shown. Notice a small MoO_x NP in the upper right, with a diameter of 35 nm.

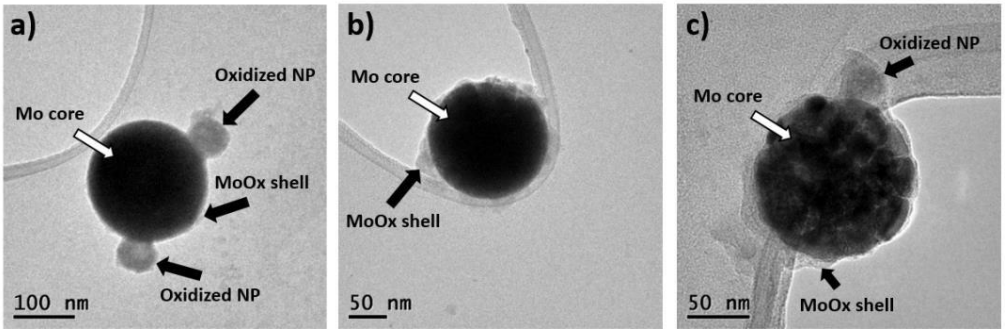

Fig 3.4 TEM images of the MoO_x NPs

With the help of the images obtained with the TEM microscope, we were able to identify three types of generated MoO_x NPs. Large (141 ± 12 nm) Mo NPs which are covered by a tiny molybdenum oxide layer, medium (97 ± 7 nm) sized NPs with a thicker layer of molybdenum oxide around a smaller core, and finally small (48 ± 4 nm) Mo NPs which form large quasi-spherical agglomerates. In the last case one can see abundant molybdenum oxide covering the agglomerate. In all three cases presented in figure 3.4, the

core-shell type of structure is evident. Similar structures have been reported forming MoC@grafite NPs by using ps laser pulses [33].

By utilizing the TEM images, we measure the NPs diameter and plot the size distribution, figure 3.5. In 3.5 a), b) and c), it can be seen as expected that the average of the diameter of the MoO_x NPs increase as the energy of laser irradiation rises for 5, 10 and 15 J/cm^2 [25]. Actually, the average diameter of the NPs obtained with 10 and 15 J/cm^2 is almost twice and three times the size of the NPs generated with 5 J/cm^2, just like the augmentation of energy, respectively.

A Gaussian size distribution is appreciated in figure 3.5 b) and c), similar curve shapes have been reported for Ge [34] and Si [35] NPs synthesized with ps laser pulses. For d) 20 J/cm^2 the averaged diameter of the NPs does not follow the linear relation seen for lower energies and size. The average diameter of the NPs formed at this energy is smaller than the one obtained for 15 J/cm^2. This may occur because of the interaction of the beam with the large NPs, which causes its fragmentation [35].

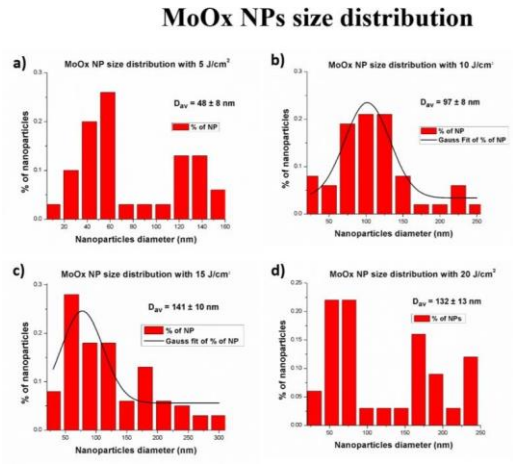

Fig 3.5 Size distribution of the NPs obtained with a) 5 J/cm^2, b) 10 J/cm^2, c) 15 J/cm^2 and d) 20 J/cm^2.

3.3.3 Proposed mechanism of the Mo@MoOx NPs formation (aging effect)

A schematic hypothesis of the molybdenum oxidation process is shown in figure 3.6 Right after the formation of the Mo NPs, they interact with the liquid media. The water molecules oxidize the surface of the Mo NPs that have been created, as time passes the surface of the NPs keeps oxidizing since they are still submerged in the aqueous suspension; after several weeks the initial NPs evolve into either pure MoO_x or $Mo@MoO_x$ in core-shell type NPs, this may depend on the initial size of the NP.

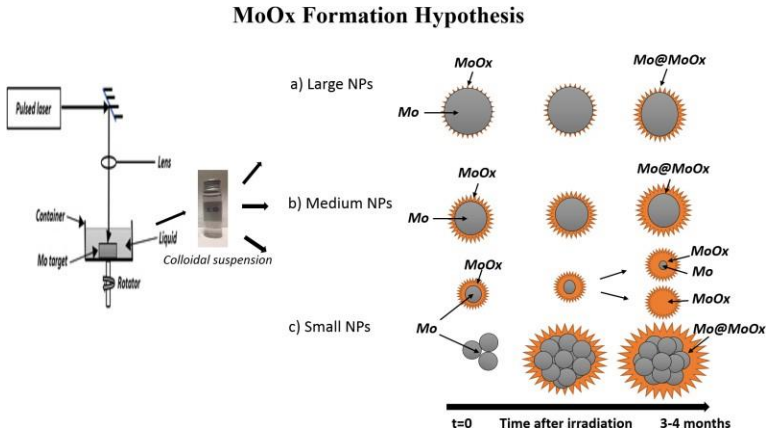

Fig 3.6 MoO_x NPs colloidal suspension aging process hypothesis.

The NPs generated have diameters from tens to a few hundreds of nm. Figure 3.5a) illustrates the aging process for large NPs; since large NPs are chemically more stable than medium and small ones due to the surface to volume ratio [36], they experience less oxidation and the average thickness of the oxide layer is smaller as compared to the one formed on medium and small NPs. For medium size NPs (figure 3.5b) the oxide layer is

considerable thicker than the one found in large NPs. In the case of small NPs (figure 3.5c) right after been formed, two scenarios may take place due to their chemical instability. Some of the small NPs get attached to the surface of larger NPs, where they undergo oxidation; some others tend to form big agglomerates in order to achieve a more stable structure, still this agglomerate sees a considerable oxide layer formation.

3.3.4 Raman spectroscopy

The Raman spectrum in figure 3.7 shows different bands which are associated with molybdenum oxide hydrates ($MoO_3 \cdot xH_2O$) (x = 1, 2) [37]. These compounds structure come from the presence of MoO_5 (OH_2) octahedral sharing either corner equatorial oxygens or edges that exhibit different vibration modes. It can be seen two strong and broad bands, one at 245 cm^{-1} and another at 974 cm^{-1} that can be assigned to stretching vibrations of OMo_3 units that correspond to $MoO_3 \cdot H_2O$. A weak signal at 350 cm^{-1}, which is associated with $MoO_3 \cdot 2H_2O$ described as the νMo-OH_2 stretching vibrations. The band at 620 cm^{-1} is assigned to stretching vibrations of OMo_3 units that correspond to $MoO_3 \cdot H_2O$. Finally, at 865 cm^{-1} there is a small band that may be related to the bridging oxygens linked to two metal atoms in two dimensional arrangements corresponding to $MoO_3 \cdot 2H_2O$ [37].

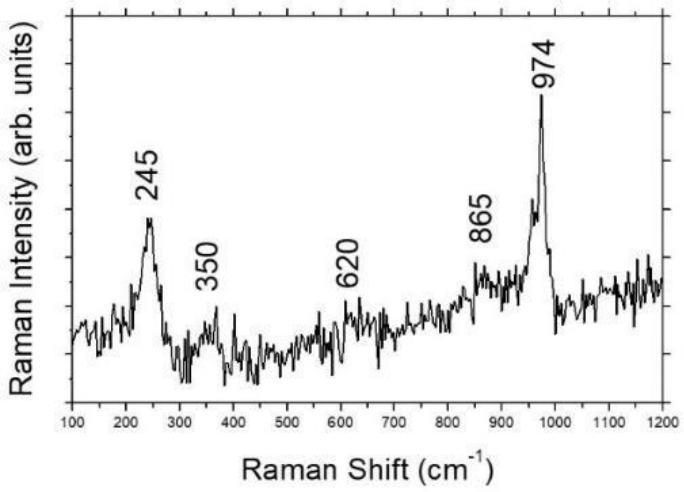

Fig 3.7. Raman spectra of the hydrated molybdenum trioxide obtained.

3.4 Conclusions

This work presents the generation of spherical Mo@MoO_x NPs by using the LASL technique with potential application in energy systems or as photonic material. The average sizes are 48, 97, 141 and 132 nm obtained with laser fluences of 5, 10, 15 and 20 J/cm^2, respectively. The UV-Vis spectroscopy analysis showed that the colloidal suspension evolves in time, as a result of aging the absorbance increases. TEM images show the formation of three different types of NPs. Raman spectra shows that the NPs are composed of $MoO_3 \cdot xH_2O$, with x= 1, 2. Further studies are being conducted to synthesize MoO_x NPs that exhibit absorbance in the optical biological window in order to use them as potential photothermal agents.

References

[1] J. Dowden, The theory of laser materials processing, 1st ed. Springer series in materials science; 2008.

[2] Simakin, A.V., Voronov, V.V. & Shafeev, G.A, Nanoparticle formation during laser ablation of solids in liquids, Phys. Wave Phen. 15 (2007) 218. https://doi.org/10.3103/S1541308X07040024

[3] S. I. Dolgaev , A. V. Simakin , V. V. Voronov , G. A. Shafeev , F. Bozon-Verduraz , Nanoparticles produced by laser ablation of solids in liquid environment. Appl. Surf. Sci., 186 (2002) 546. https://doi:10.1016/s0169-4332(01)00634-1.

[4] V. Amendola, M. Meneghetti, What controls the composition and the structure of nanomaterials generated by laser ablation in liquid solution? Phys. Chem. Chem. Phys. 15 (2013) 3027-3046. https://doi10.1039/C2CP42895D.

[5] H. Zeng, X.D. Du, S.C. Singh, S.A. Kulinich, S. Yang, J. He, W. Cai, Nanomaterials via Laser Ablation/Irradiation in Liquid: A Review, Adv. Funct. Mater. 22 (2012) 1333–1353. https://doi:10.1002/adfm.201102295.

[6] P. S. Liu , W. P. Cai , H. B. Zeng, Fabrication and size-dependent optical properties of FeO nanoparticles induced by laser ablation in a liquid medium, J. Phys. Chem. C. 112 (2008) 9, 3261-3266. https://doi:10.1021/jp709714a.

[7] T. X. Phuoc , B. H. Howard , D. V. Martello , Y. Soong , M. K. Chu, Synthesis of Mg(OH)2, MgO, and Mg nanoparticles using laser ablation of magnesium in water and solvents, Optics and Lasers in Engineering 46 (2008) 829– 834. https://doi.org/10.1016/j.optlaseng.2008.05.018.

[8] S. Dadashi, R. Poursalehi, H. Delavari H, "Formation, gradual oxidation mechanism and tunable optical properties of Bi/Bi2O3 nanoparticles prepared by Nd:YAG laser ablation in liquid: Dissolved oxygen as genesis of tractable oxidation", Materials Research Bulletin 97 (2018) 421–427.

[9] I. Rocha-Mendoza, S. Camacho-López, Y. Luna-Palacios, Y. Esqueda-Barrón, M. A. Camacho-López, M. Camacho-López, G. Aguilar, "Second- harmonic generation of ZnO nanoparticles synthesized by laser ablation of solids in liquids", *Optics and Laser Technology*, 99 (2018) 118–123.

[10] Yi-Pei Lee, Yi-Hsin Liu and Chen-Sheng Yeh, "Formation of bayerite, gibbsite and boehmite particles by laser ablation", *Phys. Chem. Chem. Phys*., 1999, 1, 4681È4686.

[11] J Haber, Lalik HE, Catalytic properties of MoO_3 revisited, Catalysis Today, 33 (1993): 1-3 119-137. https://doi:10.1016/S0920-5861(96)00107-1.

[12] Scarminio J, Lourenco A, Gorenstein A, Electrochromism and photochromism in amorphous molybdenum oxide films, Thin Solid Films 302 (1997) 66-70. https://doi.org/10.1016/S0040-6090(96)09539-9.

[13] Y. Zhan, Y. Liu, H. Zu, Y. Guo, S. Wu, H. Yang, Z. Liu, B. Lei, J. Zhuang, X. Zhang, D. Huang and C. Hu, Phase-controlled synthesis of molybdenum oxide nanoparticles for surface enhanced Raman scattering and photothermal therapy, Nanoscale, 10 (2018) 5997-6004. https://doi.org/10.1039/C8NR00413G.

[14] Song G1, Shen J, Jiang F, Hu R, Li W, An L, Zou R, Chen Z, Qin Z, Hu J, Hydrophilic molybdenum oxide nanomaterials with controlled morphology and strong plasmonic absorption for photothermal ablation of cancer cells, ACS Appl. Mater Interfaces. 6 6 (2014) 3915-22. https://doi:10.1021/am4050184.

[15] M. Cano-Lara, S. Camacho-López, A. Esparza-García, M.A. Camacho-López, Laser-induced molybdenum oxide formation by low energy (nJ)–high repetition rate (MHz) femtosecond pulses, Optical Materials 33 (2011) 1648– 1653. https://doi.org/10.1016/j.optmat.2011.04.029.

[16] M. A. Camacho-López , L. Escobar-Alarcón, M. Picquart, R. Arroyo, G. Córdoba, E. Haro-Poniatowski, Micro-Raman study of the m-MoO2 to a- MoO_3 transformation induced by cw-laser irradiation, Optical Materials 33 (2011) 480–484. https://doi.org/10.1016/j.optmat.2010.10.028.

[17] C. Julien, A. Mauger, A. Vijh, K. Zaghib, Lithium Batteries: Science and Technology, Springer International Publishing, 1st ed., 2016. https://doi.org/10.1007/978-3-319-19108-9.

[18] P. F. Carcia, E. M. McCarron III, Synthesis and properties of thin film polymorphs of molybdenum trioxide, Thin Solid Films, 155 (1987) 53-63, https://doi.org/10.1016/0040-6090(87)90452-4

[19] T. Pham, P. Nguyen, T. Vo, H. Nguyen and C. Luu, Facile method for synthesis of nanosized β–MoO_3 and their catalytic behavior for selective oxidation of methanol to formaldehyde, Adv. Nat. Sci.: Nanosci. Nanotechnol. 6 (2015) 045010 6. https://doi:10.1088/2043-6262/6/4/045010.

[20] D. O. Scanlon, G. W. Watson, D. J. Payne, G. R. Atkinson, R. G. Egdell, S. L. Law, Theoretical and Experimental Study of the Electronic Structures of $MoO_3$and MoO_2, J. Phys. Chem. C, 114 10 (2010) 4636-4645. https://doi:10.1021/jp9093172.

[21] I. Alves de Castro, R. Datta, J. Ou, A. Castellanos-Gomez, S. Sriram, T. Daeneke, and K. Kalantar-zadeh, Molybdenum Oxides – From Fundamentals to Functionality, Adv. Mater. 29 (2017) 1701619. https://doi:10.1002/adma.201701619.

[22] Maaza, M., Ngom, B.D., Khamlich, S, Valency control in $MoO_{3-\delta}$ nanoparticles generated by pulsed laser liquid solid interaction, J Nanopart Res., 14 (2012) 714. https://doi.org/10.1007/s11051-011-0714-3.

[23] V. T. Karpukhin, M. M. Malikov, M. V. Protasov, T. I. Borodina, G. E. Val'yano, and O. A. Gololobova, Composition, morphology characteristics, and optical properties of molybdenum oxide nanostructures synthesized by the laser ablation method in liquid, High Temp 55 (2017) 870. https://doi.org/10.1134/S0018151X17060098.

[24] S. Spadaro1, M. Bonsignore, E. Fazio, F. Cimino, A. Speciale, D.Trombetta, F. Barreca, A. Saija, F. Neri, Molybdenum oxide nanocolloids prepared by an external sield-assisted laser ablation in water, EPJ Web of Conferences, 167 (2018) 04009. https://doi.org/10.1051/epjconf/201816704009.

[25] V. Amendola, M. Meneghetti, Laser ablation synthesis in solution and size manipulation of noble metal nanoparticles, Phys. Chem. Chem. Phys., 11 (2009) 3805-3821. https://doi.org/10.1039/B900654K.

[26] Ayi A, Chinyere A. Anyama, and Varsha K, On the Synthesis of Molybdenum Nanoparticles under Reducing Conditions in Ionic Liquids, Journal of Materials, 372716 (2015) 1–7. http://dx.doi.org/10.1155/2015/372716.

[27] J. Shi, Y. Kuwahara, M. Wen , M. Navlani- García, K. Mori, T. An, H. Yamashita, Room-temperature and aqueous-phase synthesis of plasmonic molybdenum oxide nanoparticles for visible-light-enhanced hydrogen generation, Chem. Asian J. 00 (2016) 0–0. https://doi: 10.1002/asia.201600771.

[28] Jeffrey M. McMahon,wab George C. Schatza and Stephen K. Gray, Plasmonics in the ultraviolet with the poor metals Al, Ga, In, Sn, Tl, Pb, and Bi, Phys. Chem. Chem. Phys., 15 (2013) 5415-5423. https://doi10.1039/C3CP43856B.

[29] S. H. Lee, H. Nishi and T. Tatsuma, Tunable plasmon resonance of molybdenum oxide nanoparticles synthesized in non-aqueous media, Chem. Commun., 53 (2017) 12680-12683. https://doi10.1039/C7CC08090E.

[30] Ding D, Guo W, Guo C, Sun J, Zheng N, Wang F, Yan M, Liu S, MoO3- x quantum dots for photoacoustic imaging guided photothermal/photodynamic cancer treatment. Nanoscale, 9 (2017) 2020- 2029. https://doi10.1039/C6NR09046J.

[31] Y. Yang, Y. Yang, S. Chen, Q. Lu, L. Song, Y. Wei and X. Wang, Atomic-level molybdenum oxide nanorings with full-spectrum absorption and photoresponsive properties, Nature communications, 8 (2017) 1559. https://doi10.1038/s41467-017-00850-8.

[32] S. Dadashi, R. Poursalehi, H. Delavari, Optical and structural properties of Bi-based nanoparticles prepared via pulsed Nd:YAG laser ablation in organic liquids, *Applied Physics A*, 124 (2018) 406. https://doi.org/10.1007/s00339-018-1817-9.

[33] M. Madrigal-Camacho, A. R. Vilchis-Nestor, M. Camacho-Lopez, M. A. Camacho-Lopez, Synthesis of MoC@Graphite NPs by short and ultra- short pulses laser ablation in toluene under N_2 atmosphere. Diamond & Related Materials, 82 (2018) 63–69. https://doi.org/10.1016/j.diamond.2017.12.019.

[34] M. Rodio, A. Scarpellini, A. Diaspro and R. Intartaglia, Tailoring of size, emission and surface chemistry of germanium nanoparticles via liquid-phase picosecond laser ablation, J. Mater. Chem. C, 5 (2017) 12264-12271. https://doi.org/10.1039/C7TC01992K.

[35] R. Intartaglia, K. Bagga, and F. Brandi, Study on the productivity of silicon nanoparticles by picosecond laser ablation in water: towards gram per hour yield, Opt. Express 22 (2014) 3117-3127. https://doi.org/10.1364/OE.22.003117.

[36] S. Eustis and M. A. El-Sayed, Why gold nanoparticles are more precious than pretty gold: Noble metal surface plasmon resonance and its enhancement of the radiative and nonradioactive properties of nanocrystals of different shapes, Chem. Soc. Rev., 35 (2006) 209-217. https://doi.org/10.1039/B514191E.

[37] L. Seguin, Infrared and Raman spectra of MoO_3 molybdenum trioxides and $MoO_3 \cdot xH_2O$ molybdenum trioxides hydrates, Spectrochimica Acta, 51 (1995) 1323-1344. https://doi.org/10.1016/0584-8539(94)00247-9.

Chapter 4 Synthesis of Molybdenum Oxide Nanoparticles by Nanosecond Laser Ablation

4.1 Introduction

PTT has shown remarkable results for selective tumor ablation, some of the advantages of this therapy are that it is noninvasive and relatively easy to perform [1-4]. Finding the most suitable PTT agent is essential for the progress and possible implementation of this therapy in clinical trials, nevertheless it has been and still a challenge for researchers because of the peculiar properties a PTT agent must possess. Noble nanomaterials have been the most explored so far, especially the ones made of Au [5-8]. However, its practical application is limited by their high cost, and other materials are being considered [9-11].

In recent years one of the most attractive materials for a wide range of potential applications, ranging from optical and electronic to energy and bio devices is MoO_x [12-24]. Some of these oxides exhibit surface plasmon resonance (SPR) across different spectral regions; this enables optical tunability, which permits the synthesis of nanostructures (NS) that absorb light in the near infrared (NIR), where light has the deepest penetration in biotissue [17- 24]. In fact, different MoO_x NS have been used as PTT agents with very promising results, since these materials have shown low toxicity, strong NIR absorption and photothermal conversion efficiency [20-24].

Different groups have synthesized MoO_x NS using chemical synthesis methods. For instance, Yin, *et al*., reported PEG-MoO_x NPs that exhibit broad absorption in the NIR

region and strong photothermal conversion ability, they showed these NPs can be used to treat tumors by synergetic PTT and photodynamic therapy (PDT) in *in vitro* experiments [21]. Liu, *et al*., obtained chemical highly stable MoO_2 bow tie-like NPs by using a hydrothermal method as well, and showed they could withstand high temperature heating without oxidation and have a SPR effect from visible to NIR [22].

Furthermore, Zhan, *et al*., synthesized low cost and stable MoO_2 NPs with tunable phase by using a solvothermal method and found that the photothermal conversion efficiency as high as 61.3%, this was attributed to the large amount of free electrons provided by the sufficient concentration of oxygen vacancies [23]. Besides, Song, *et al*., generated hydrophilic molybdenum trioxide MoO_3-Poly- ethylene-glycol (PEG) nanospheres and nanoribbons by using a hydrothermal method and reported these NS to have a strong SPR in the NIR region and can be used in hyperthermia therapy [24].

On the other hand, the LASL method has shown to be successful for synthesizing a big variety of NS [25-33] including MoO_x NS [30-33]. Some of the advantages of this technique are that it is a straightforward, one-step and clean synthesis method, since it produces reduced or nonexistent byproducts and there is no need for catalyst. These NS are generated in ambient conditions, not extreme temperature or pressure are needed and some properties of the synthesized NS (shape, size distribution) can be conveniently controlled upon LASL by conveniently adjusting the laser parameters or changing the type of liquid medium. [35-36] In [30], core shell-type MoO_x NS with average sizes from 48 to 141 nm were synthesized by picosecond LASL. The absorption spectra of the colloidal solution showed a peak around 210 nm and a shoulder around 240 nm. An oxidation process

of the NS due to aging was proposed. In [31], nickel-molybdenum alloys were generated by ns LASL. An absorption peak at about 215 nm and a shoulder at 240 nm, which correspond to MoO_3 NPs was found. It was also reported that after few weeks two absorption bands appeared from 500 to 900 nm.

However, in spite of the great potential application of the MoO_x NS as PTT agents in one hand, and the versatility and popularity of LASL one the other, this type of NS have never been synthesized with these properties with ns pulses as far as we know. This is the motivation of our present work, where we report on the generation of core-shell type MoO_x by the LASL method.

The NPs obtained are free of surfactants or additives and exhibit absorbance in the so called optical biological window around 840 nm, which makes them suitable as PTT agents. They were obtained by ablating a Mo target submerged in deionized water, with a ns laser for either 30 minutes or 20 minutes plus 10 more of colloidal irradiation; the last was performed with the purpose of studying NPs fragmentation. TEM-EDX scans show a core-shell type NS formation, the band gaps were calculated by using Tauc's rule with values of 4.1 eV and 4.2 eV and micro-Raman studies indicate these NPs are composed of molybdenum trioxide hydrates ($MoO_3 \cdot xH_2O$).

4.2 Experimental

4.2.1 Synthesis of the Mo NPs colloidal suspensions

A nanosecond (ns) Nd:YAG (continuum minilite) pulsed laser and a highly pure (99.95 %) Mo target disk (*Kurt J, Lesker Co*) with a 7 mm depth were usedto synthesize the NPs. The target was submerged in 6 ml of DI water, forming a 1 cm height column from the surface.Then it was irradiated with a beam of 25 mJ, focused with a 200 mm focal lens forming a 27.5 mm diameter beam on the material surface. The per pulse laser fluence and laser repetition rate frequency were kept constant. The experiments were performed at room temperature with not external extreme tempearature or pressure were needed. (fig. 1).

To study the effect of fragmentation on the NPs properties, two experiments were carried out. The idea was to keep all parameters constant but the time of target irradiation. In the first one, the target was continuously ablated for 30 minutes. In the second one, the same target was ablated for 20 minutes, then it was taken out of the container and the generated colloidal solution was irradiated for 10 minutes to induce fragmentation. The pulse length was 7 ns and its fluence was 4.2 mJ/cm^2, the laser pulses were delivered at 10 Hz and a wavelength of 1,064 nm. The Mo target was rotating while ablating in order to avoid irradiation of the same target spot.

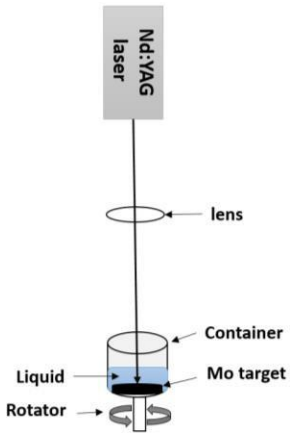

Fig 4.1. Shows a schematic of the LASL experimental set up used to synthesize the MoO_X NPs.

4.3 Sample characterization

4.3.1 UV-Vis characterization

A double beam spectrometer (Lambda 650 Perkin-Elmer) with range spanning from 200 to 900 nm was utilized to carry out the optical characterization of the obtained colloidal suspensions. A quartz cuvette with an optical path length of 10 mm was used, the optical absorption spectra measurements were taken three days after the NPs synthesis.

4.3.2 Transmission electron microscopy-Energy-dispersive X-ray

The morphology, size and structure studies of the Mo NPs were performed on a Transmission Electron Microscope-EDX (JEM 2100 from JEOL) operated at 120 kV accelerating voltage equipped with a LaB_6 filament. For ample preparation, a drop of the NPs suspension was placed on a lacey-carbon Cu grid, it was allow to evaporate at room

conditions and then was observed in the TEM. In order to obtain information of the particle size and distribution, the dimensions of many particles were measured employing the ImageJ™ software.

4.3.3 Raman micro-spectroscopy

Raman spectra were recorded by using a micro-Raman Horiba Jobin Yvon system, model Xplora plus. A solid-state laser at 532 nm with a nominal power of 25 mW was used to generate the Raman signal. A 100x objective lens was used to focus the laser beam and also served the purpose of collecting the scattered light. The delivered laser power on the sample surface was 1% of the nominal power. A 1200 lines/mm grating was employed, 100 acquisitions were averaged with an exposure time of 1 s each one.

4.4 Results and discussion

4.4.1 Optical properties of Mo NPs colloidal suspensions

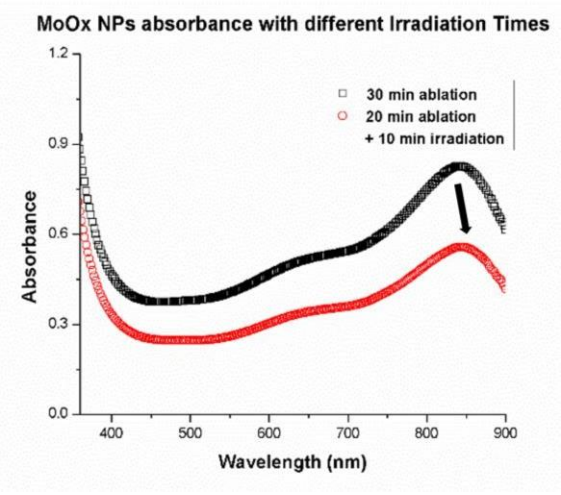

Figure 4.2. MoO_x NPs colloidal suspension absorbance spectra.

Figure 4.2 shows the absorbance of the colloidal solutions in DI water obtained by ablating the target with 4.2 J/cm^2 for 30 min and 20 min plus 10 min of irradiation. It can be seen on both spectra that the value of the absorbance is relatively high for wavelengths below 400 nm, this is related to metallic Mo NPs [37]. There is a peak at around 840 nm, which is attributed to the formation of MoO_x NPs in this size range -tenths of nanometers- similar spectra have been obtained for MoO_x NPs with similar diameters by chemical methods [21].

Moreover, even though both spectra look very similar, there are two subtle but important differences. On the one hand, the value of the absorbance is clearly higher for the colloidal solution obtained with 30 minutes of constant ablation (black squares), this is due to the fact that the solution is more concentrated since longer times of ablation produce a larger amount of NPs [34-36].

On the other hand, the absorbance peak for the colloidal solution obtained with 20 minutes of ablation plus 10 minutes of irradiation (red triangles) is slightly red shifted, it is located at around 845 nm, marked with a black arrow. The last is explained by NPs fragmentation produced by the extra irradiation time of the colloidal solution. It is well-known from the Mie scattering theory that the optical properties of nanostructures are directly related to its size [38].

Having NPs that exhibit an absorption peak in the NIR range is mandatory for the purpose of using them as PTT agents. NIR light penetrates deep in biotissue, this is why finding an absorbance peak at around 840 nm in this work is remarkable, especially because it has never been reported when synthesizing MoO_x NPs with suitable sizes for PTT by

LASL with ns pulses. Another significant result is demonstrating the NPs synthesis free of surfactants, additives or any chemical pollutant as opposite to most chemical methods [21-24].

4.4.2 Band Gap estimation

In order to estimate the energy band gap of the NS synthesized, the data from UV-Vis absorption and Tauc's rule were used [39, 40].

$$(\alpha h\nu)^{1/n} \approx (h\nu - {}_{g}E)$$

Where α is the absorption coefficient, h is Plank's constant, ν is the frequency of photon, E_g is the energy band gap and the n = ½ for a direct band gap [41-43].

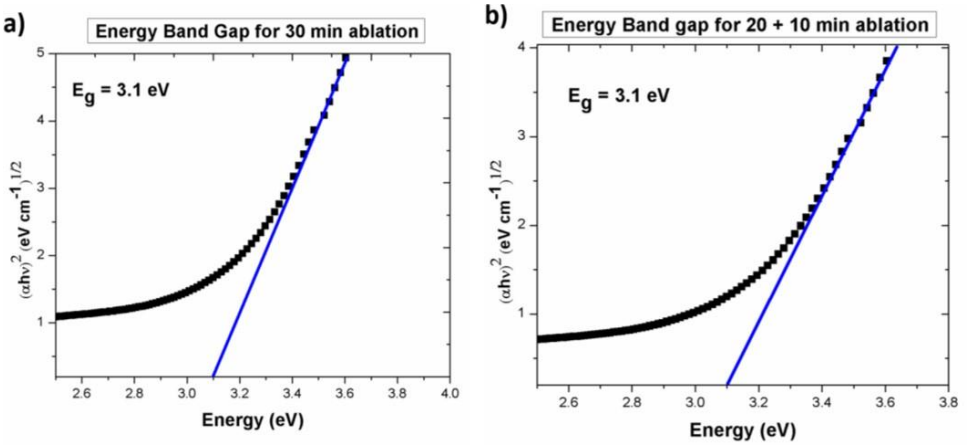

Figure 4.3. Energy band gap calculation for the colloidal solutions by using Tauc's method for a) 30 minutes ablation and b) 20 minutes ablation + 10 minutes of colloidal irradiation.

The band gap energy results are shown in figure 3. The estimated value obtained is 3.1 eV for both colloidal solutions generated either a) with 30 minutes of continuous ablation or b) 20 minutes ablation + 10 minutes colloidal irradiation, respectively, which correspond to the semiconductor MoO3 [12].

4.4.3 TEM images of the Mo NPs

Representative TEM micrographs of the MoO_x NPs obtained and corresponding size distribution graphs for the two experiments are shown in figure 4. Figure 4a), b) and c)shows images corresponding to the continuous ablation of the Mo target for 30 minutes. Figure a) shows core-shell type NPs with sizes from 20 and up to 100 nm; particularly in the largest one, marked with arrows it can be seen that the Mo core looks darker, since it is denser than the MoO_x shell that surrounds it, which looks light grey [29]. In figure b) semi spherical NPs with various sizes are seen in a different scale, these NPs were obtained under the same laser irradiation parameters. The graph in figure 4c) shows that the size range spans from 6.5 to 100.3 nm and it has a bimodal size distribution with peaks at 25 nm and 90 nm.

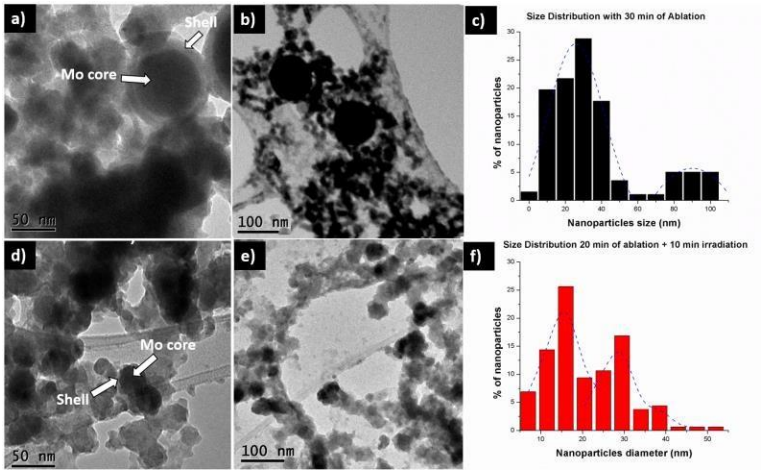

Fig 4.4. TEM images of MoO_X NPs obtained and their corresponding size distribution graphs when ablating the Mo target for 30 minutes continuously in figure a), b) and c), and for 20 minutes plus 10 minutes of irradiation of the colloidal solution in d), e) and f).

Figure 4d) show representative images of the MoO_x NPs obtained with 20 minutes of ablation plus 10 minutes of colloidal solution irradiation.In figure 4d), we can see semispherical core-shell type NPs of various sizes in a different scale, obtained under the same laser irradiation parameters. Finally, the graph in figure 4f) shows that the size range spans from 7 to 52 nm andit also has a bimodal size distribution with peaks at 16 and 28 nm.

During laser irradiation of the colloidal solution, NPs absorbed energy and their temperature promptly approaches the melting point, which causes them to fragment [44].The effect of inducing NPs fragmentation, by irradiating the colloidal solution after removing the target, is clearly seen when comparing the size distribution of the two samples. For instance, it can be seen that the size peak of 4c) is 25 nm compared to 16 nm in the figure 4f), correspondly the second peak is around 90 nm whereas in the latter is reduced to 28 nm. A plausible explanation for this is that the absorption coefficient is larger for larger NPs [44]. These size reduction was expected and it is in agreement with other reports for other materials synthesized by LASL with similar irradiation parameters. Obtaining a bimodal size distribution is common when synthesizing NS with ns pulses and the two possible responsible explanations for this are thermal vaporization and explosive intensity boiling [26, 35, 36].

4.4.4 TEM- EDX images of the Mo NPs

The elemental distribution of the NS generated was studied by using TEM- EDX images and two elements were found.

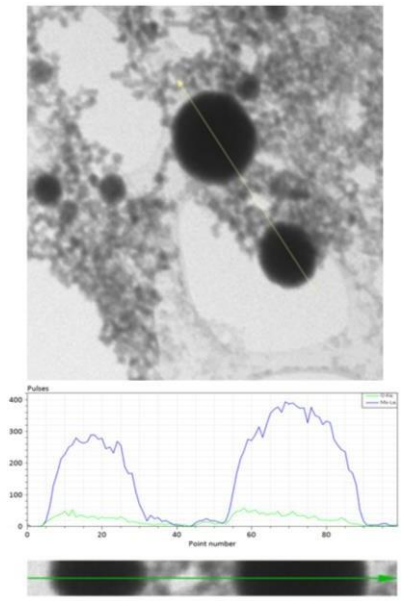

Fig 4.5. TEM-EDX images of MoO_X NPs obtained with 30 minutes of continues ablation.

Figure 5 shows representative EDX line scans images, it can be seen in both NPs scanned that they are composed mainly of molybdenum and some oxygen, and the elemental distribution correspond to a core-shell type NS [45, 46], in which the core is made of metallic molybdenum shown with a blue line in the spectra, and it is surrounded by molybdenum oxide which corresponds to the superposition of blue and green lines in the spectra, as proposed in [30].

4.4.5 Raman spectroscopy

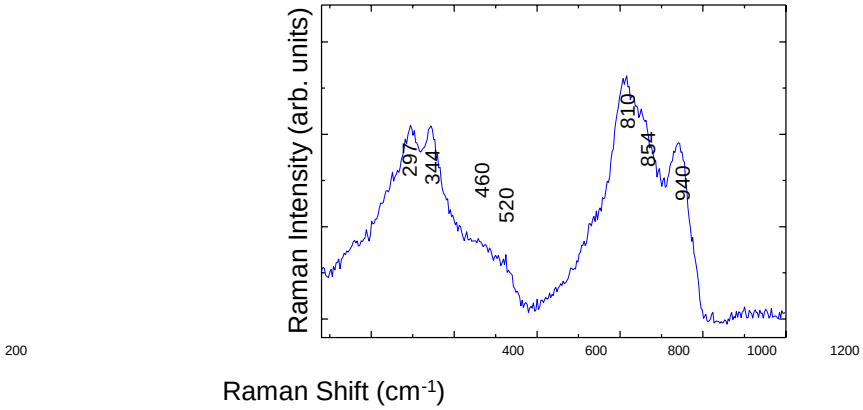

Fig 4.6. Raman spectrum of the obtained hydrated molybdenum trioxide.

The formation of oxides may be generated when ablated species react with dissolved molecular or water bound oxygen deliberated simultaneously by the photothermal decomposition of the water when plasma is cooling [31]. The obtained Raman spectrum for the samples irradiated for 30 minutes is shown in figure 6, the one obtained for 20 minutes ablation plus 10 minutes of colloidal irradiation was almost identical and for space reasons it is not shown.

The different bands are associated with molybdenum oxide hydrates ($MoO_3 \cdot H_2O$) [47-49]. These compounds structure comes from the presence of MoO_5 (OH_2) octahedral, sharing either corner equatorial oxygens or edges that exhibit different vibration modes. A broad band can be seen in the left part of the spectrum from 297 to 460 cm^{-1}, which might correspond to several νMo-OH_2 vibrations, coming from several Mo-H_2O distances and/or dipolar coupling between several of such oscillations. A weak signal at 520 cm^{-1} can be identified, which is related to the stretching vibration of O-Mo3 units.

In the right part of the spectrum, there are two strong signals. The first peak at 810 cm^{-1} might come from the stretching vibrations of Mo3-O-Mo3 units, which is related to α-MoO_3. The second peak at 854 cm^{-1} is located in a spectral range where stretching vibrations are associated to Mo-O bonds corresponding to β- MoO3. Finally, there is a broad peak at 940 cm^{-1} which is described as the νOH=Mo stretching vibration unit [47-49].

4.5 Conclusions

This work reports the generation of MoOx NPs by using the LASL method with ns laser pulses. The produced NPs show potential as PTT agents. The synthesis of these NPs is surfactants/additives free. Remarkably, these MoOx NPs possess an absorption peak in the optical biological window, this peak is located at around 840 nm and size peaks from 16 to 90 nm, which makes them suitable for PTT. The TEM-EDX images demonstrate core-shell type NPs with elemental composition of molybdenum and molybdenum oxide, and bimodal sizes with peaks at 25 and 90 nm, and 16 and 28 nm for ablation of 30 minutes and 20 minutes ablation + 10 minutes of colloidal irradiation, respectively.

As a result of the NPs laser-induced fragmentation the NPs size decreases. As a consequence the absorption peak is slightly red shifted. The generated and are composed of a metallic Mo core, and the micro-Raman study shows that the shells are constituted of amorphous molybdenum oxide hydrates (MoO3 · xH2O). The calculated energy band gap is 3.1 eV which corresponds to MoO3. Future research is being conducted to set the irradiation parameters for optimizing the NPs absorbance in the NIR range and carry out hyperthermia studies with cw irradiation.

Acknowledgments

This work was possible thanks to the UCMEXUS-Conacyt scholarship for doctoral studies awarded to Noe Zamora-Romero. TEM facilities were financial supported by CONACyT-México (Grant No. 280518)

All authors claim not to have conflict of interest related to this article.

References

[1] D. P. O´Neal, L.R Hirsch, N.J. Halas, J.D Payne, J.L. West, Photo-thermal ablation in mice using near infrared-absorbing nanoparticles. Cancer Letters 209 (2004) 171-176. https://doi.org/10.1016/j.canlet.2004.02.004

[2] I. H. El-Sayed, X. Huang, M. A. El-Sayed, Selective laser photo-thermal therapy of epithelial carninoma using anti-EFGR antibody conjugated gold nanoparticles. Cancer letter 239 (2006) 129-135. https://doi.org/10.1016/j.canlet.2005.07.035

[3] C. Loo, A. Lowery, N. Halas, J. West, R. Drezek, Inmunotargeted nanoshells for integrated cancer imaging and therapy. Nano letters 5. 4. (2005) 709-711. https://doi10.1021/nl050127s

[4] S. Lal, P. K. Clare, N. J. Halas, Nanoshell-enabled photothermal cancer therapy: impeding clinical impact. Accounts of Chemical Med. Sci. 23 (2008) 217-228. https://doi 10.1021/ar800150g

[5] X. Huang, P. K. Jain, I. H. El-Sayed, M. A. El-Sayed, Plasmonic photothermla therapy using gold nanoparticles. Lasers Med. Sci 23 (2008) 217-228. . https://doi10.1007/s10103-007-0470-x

[6] T. Niidome, M. Yamagata, Y. Okamoto, Y. Akiyama, H. Takahashi, T. Kawano, Y. Katayama, Y. Niidome, PEG-modified gold nanaorods with a stealth character for *in vivo* applications. J. of Controlled Release. 114 (2006) 343-347. https://doi10.1016/j.jconrel.2006.06.017

[7] N. S. Abadeer and C. J. Murphy, Recent progress in cancer thermal therapy using gld nanoparticles. J. Phys. Chem. C 120 (2016) 4691-4716. . https://doi:10.1021/acs.jpcc.5b11232

[8] N. Zamora-Romero, V. Robles, C. Alvarez, N. Cuando-Espitia, L. F. Devia-Cruz, E. Penilla, D. L. Halaney, and G. Aguilar. Laser-excited gold nanoparticles for treatment of cancer cells in vitro. Medical Laser Applications and Laser-Tissue Interactions VIII, L. Lilge, ed., SPIE Proceedings 10417 (2017) 1041707. https://doi.org/10.1117/12.2286005

[9] F. Zhou, D. Xing, Z. Ou, B. Wu, D. E. Resaco, W. R. Chen, Cancer photothermal therapy in the near-infrared region by using single wall carbon nanotubes. Journal of Biomedical Optics. 14. 2 (2009) 021009. https://doi10.1117/1.3078803

[10] M. S. Mohamed, A. C. Poulose, S. Veeranarayanan, R. R. Aburto, T. Mitchman, Y. Susuky, Y. Sakamoto, P. M. Ajayan, R. R. Bouchard, Y. Yoshida, T. Maekawa, D. S. Kumar. Plasmonic fluorescence CdSe/Cu2 S hybrid nanocrystals for multichannel imaging and cancer directed photo-thermal therapy. 14.2 (2009) 021009. https://doi.org/10.1039/c5nr05225d

[11] X. Song, H. Gong, S. Yin, L. Cheng, C. Wang, Z. Li, Y. Li, X. Wang, Z. Liu. Ultra-small Iron oxide doped polypyrrole nanoparticles for in vivo multimodal guided photothermal therapy. Adv. Funct. Mater. 24 (2014) 1194-1201. https://doi.org/10.1002/adfm.201302463

[12] I. Alves de Castro, R. Datta, J. Ou, A. Castellanos-Gomez, S. Sriram, T. Daeneke, and K. Kalantar-zadeh, Molybdenum Oxides – From Fundamentals to Functionality, Adv. Mater. 29 (2017) 1701619. https://doi:10.1002/adma.201701619.

[13] T. Pham, P. Nguyen, T. Vo, H. Nguyen and C. Luu, Facile method for synthesis of nanosized β–MoO3 and their catalytic behavior for selective oxidation of methanol to formaldehyde, Adv. Nat. Sci.: Nanosci. Nanotechnol. 6 (2015) 045010 6. https://doi:10.1088/2043-6262/6/4/045010.

[14] M. A. Camacho-López , L. Escobar-Alarcón, M. Picquart, R. Arroyo, G. Córdoba, E. Haro-Poniatowski, Micro-Raman study of the m-MoO2 to a-MoO3 transformation induced by cw-laser irradiation, Optical Materials 33 (2011) 480– 484. https://doi.org/10.1016/j.optmat.2010.10.028.

[15] M. Cano-Lara, S. Camacho-López, A. Esparza-García, M.A. Camacho-López, Laser-induced molybdenum oxide formation by low energy (nJ)–high repetition rate (MHz) femtosecond pulses, Optical Materials 33 (2011) 1648–1653. https://doi.org/10.1016/j.optmat.2011.04.029.

[16] S. H. Lee, H. Nishi and T. Tatsuma, Tunable plasmon resonance of molybdenum oxide nanoparticles synthesized in non-aqueous media, Chem. Commun., 53 (2017) 12680-12683. https://doi10.1039/C7CC08090E.

[17] Ding D, Guo W, Guo C, Sun J, Zheng N, Wang F, Yan M, Liu S, MoO3-x quantum dots for photoacoustic imaging guided photothermal/photodynamic cancer treatment. Nanoscale, 9 (2017) 2020-2029. https://doi10.1039/C6NR09046J.

[18] J. Shi, Y. Kuwahara, M. Wen , M. Navlani- García, K. Mori, T. An, H. Yamashita, Room-temperature and aqueous-phase synthesis of plasmonic molybdenum oxide nanoparticles for visible-light-enhanced hydrogen generation, Chem. Asian J. 00 (2016) 0–0. https://doi: 10.1002/asia.201600771.

[19] Y. Yang, Y. Yang, S. Chen, Q. Lu, L. Song, Y. Wei and X. Wang, Atomic-level molybdenum oxide nanorings with full-spectrum absorption and photoresponsive properties, Nature communications, 8 (2017) 1559. https://doi10.1038/s41467-017-00850

[20] Anh Tran T1, Krishnamoorthy K, Song YW, Cho SK, Kim SJ., Toxicity of Nano Molybdenum Trioxide toward Invasive Breast Cancer Cells. ACS Appl. Mater. Interfaces 2014 64 2980-2986 https://doi10.1021/am405586d

[21] W. Yin, T. Bao, X. Zhang, Q. Gao, J. Yu, X. Dong, L. Yang, Z. Gu, Y. Zhao. Biodegradable MoO_X nanoparticles with efficient near-infrared phtothermal and photodynamic therapy at the second biological window. Nanoscale 10 (2018) 1517. https://doi10.1039/C7NR07927C

[22] W. Liu, X. Li, W Li, Q. Zahng, H. Bai, J. Li, G. Xi, Highly stable molybdenum dioxide nanoparticles with strong plasmon resonance are promising in photothermal cancer therapy. Biomaterials 163 (2018) 43-54. . https://doi10.1016/j.biomaterials.2018.02.021

[23] Y. Zhan, Y. Liu, H. Zu, Y. Guo, S. Wu, H. Yang, Z. Liu, B. Lei, J. Zhuang, X. Zhang, D. Huang and C. Hu, Phase-controlled synthesis of molybdenum oxide nanoparticles for surface enhanced Raman scattering and photothermal therapy,Nanoscale, 10 (2018) 5997-6004. https://doi.org/10.1039/C8NR00413G.

[24] Song G1, Shen J, Jiang F, Hu R, Li W, An L, Zou R, Chen Z, Qin Z, Hu J, Hydrophilic molybdenum oxide nanomaterials with controlled morphology and strong plasmonic absorption for photothermal ablation of cancer cells, ACS Appl. Mater Interfaces. 6 6 (2014) 3915-22. https://doi:10.1021/am4050184.

[25] J. Dowden, The theory of laser materials processing, 1st ed. Springer series in materials science; 2008.

[26] D. Zhang, B. Gökce and S. Barcikowski, Laser Synthesis and Processing of Colloids: Fundamentals and Applications, Chem. Rev.2017 1175 3990-4103. https://doi.org/10.1021/acs.chemrev.6b00468

[27] S. I. Dolgaev , A. V. Simakin , V. V. Voronov , G. A. Shafeev , F. Bozon-Verduraz , Nanoparticles produced by laser ablation of solids in liquid environment. Appl. Surf. Sci., 186 (2002) 546. https://doi:10.1016/s0169-4332(01)00634-1.

[28] H. Zeng, X.D. Du, S.C. Singh, S.A. Kulinich, S. Yang, J. He, W. Cai, Nanomaterials via Laser Ablation/Irradiation in Liquid: A Review, Adv. Funct. Mater. 22 (2012) 1333–1353. https://doi:10.1002/adfm.201102295.

[29] M. Madrigal-Camacho, A. R. Vilchis-Nestor, M. Camacho-Lopez, M. A. Camacho-Lopez, Synthesis of MoC@Graphite NPs by short and ultra-short pulses laser ablation in toluene under N_2 atmosphere. Diamond & Related Materials, 82 (2018) 63–69. https://doi.org/10.1016/j.diamond.2017.12.019

[30] N. Zamora-Romero, M. A. Camacho-Lopez, M. Camacho-Lopez, A. R. Vilchis-Nestor, V.H Castrejon-Sanchez, S. Camacho-Lopez, G. Aguilar, Molybdenum nanoparticles by pulsed laser ablation and effects of oxidation due to aging. Journal of Alloys and Compounds 788 (2019) 666-671. https://doi.org/10.1016/j.jallcom.2019.02.270

[31] G. Marzun, A. Levish, V. Mackert, T. Kallio, S. Barcikowski, P. Wagener, Laser synthesis, structure and chemical properties of colloidal nickel-molybdenum nanoparticles for the substitution of noble metals in heterogeneous catalysis, Journal of Colloid and Interface Science (2016), doi: http://dx.doi.org/10.1016/j.jcis. 2016.09.014

[32] Maaza, M., Ngom, B.D., Khamlich, S, Valency control in $MoO3-\delta$ nanoparticles generated by pulsed laser liquid solid interaction, J Nanopart Res., 14 (2012) 714. https://doi.org/10.1007/s11051-011-0714-3

[33] S. Spadaro1, M. Bonsignore, E. Fazio, F. Cimino, A. Speciale, D.Trombetta, F. Barreca, A. Saija, F. Neri, Molybdenum oxide nanocolloids prepared by an external sield-assisted laser ablation in water, EPJ Web of Conferences, 167 (2018) 04009. https://doi.org/10.1051/epjconf/201816704009

[34] V. Amendola, M. Meneghetti, What controls the composition and the structure of nanomaterials generated by laser ablation in liquid solution? Phys. Chem. Chem. Phys. 15 (2013) 3027-3046. https://doi10.1039/C2CP42895D

[35] V. Amendola, M. Meneghetti, Laser ablation synthesis in solution and size manipulation of noble metal nanoparticles, Phys. Chem. Chem. Phys., 11 (2009) 3805-3821. https://doi.org/10.1039/B900654K. [36] S. I. Dolgaev , A. V. Simakin , V. V. Voronov , G. A. Shafeev , F. Bozon-Verduraz , Nanoparticles produced by laser ablation of solids in liquid environment. Appl. Surf. Sci., 186 (2002) 546. https://doi:10.1016/s0169-4332(01)00634-1.

[37] Ayi A, Chinyere A. Anyama, and Varsha K, On the Synthesis of Molybdenum Nanoparticles under Reducing Conditions in Ionic Liquids, Journal of Materials, 372716 (2015) 1–7. http://dx.doi.org/10.1155/2015/372716.

[38] N. Khlebtsov, V. Bogatyrev, L. Dykman and A. Melnikov, Spectral Extinction of Colloidal Gold and Its Biospecific Conjugates. Journal of Colloid and Interface Science,180, 2, 25 (1996) 436-445. https://doi.org/10.1006/jcis.1996.0323

[39] J. S. Duque, B. M. Madrigal, H. Riascos and Y. P. Avila, Colloidal Metal Oxide Nanoparticles Prepared by Laser Ablation Technique and Their Antibacterial Test. Colloids Interfaces, 2019,3, 25. https://doi:10.3390/colloids3010025

[40] M. Shkir, Ganesh, V., Yahia, I.S. et al. J Mater Sci: Mater Electron (2018) 29: 15838. https://doi.org/10.1007/s10854-018-9670-3

[41] S. Sun, Yang, X.; Zhang, Y.; Zhang, F.; Ding, J.; Bao, J.; Gao, C. Enhanced photocatalytic activity of sponge-like ZnFe2O4 synthesized by solution combustion method. Prog. Nat. Sci. 22 (2012) 639–643. https://doi.org/10.1016/j.pnsc.2012.11.008

[42] T. Theivasanthi. Alagar, M. Lead Nanopowder as Advanced Semi-Conductor, An Insight. Res. Appl. Mater 1 (2013) 36–43. https://doi10.12966/ram.07.02.2013

[43] Baset, S. Akbar, H. Size measurement of metal and semiconductor nanoparticles via uv-vis absorptionspectra. Dig. J. Nanomater. Biostruct. 6 (2011) 709–716.

[44] A.Takami, H. Kurita, S. Koda, Laser-Induced Size Reduction of Noble Metal Particles. J. Phys. Chem. 1038 (1999) 1226-1232. https://doi.org/10.1021/jp983503o

[45] Peter Strasser, Shirlaine Koh, Toyli Anniyev, Jeff Greeley, Karren More, Chengfei Yu, Zengcai Liu, Sarp Kaya, Dennis Nordlund, Hirohito Ogasawara, Michael F. Toney & Anders Nilsson. Lattice-strain control of the activity in dealloyed core–shell fuel cell catalysts. Nature Chemistry. 2 (2010) 454–460. https://doi 10.1038/NCHEM.623.

[46] G. Yang, D. Chen, L. Pengmei, X. Kong, Y. Sun, Z. Wang, Z. Yuan, H. Liu and J. Yang Core-shell Au-Pd nanoparticles as cathode catalysts for microbial fuel cell applications. Scientific Reports. 6 (2016) 35252. https://doi.1038/srep35252

[47] L. Seguin, Infrared and Raman spectra of MoO_3 molybdenum trioxides and $MoO_3 \cdot xH_2O$ molybdenum trioxides hydrates, Spectrochimica Acta, 51 (1995) 1323-1344. https://doi.org/10.1016/0584-8539(94)00247-9

[48] M. A. Camacho-López, E. Haro-Poniatowski, L. Lartundo-Rojas, J. Livaged, M. Juliene, "Amorphous–crystalline transition studied in hydrated MoO_3", Materials Science and Engineering 135 2 25 (2006) 88- 94. https://doi.org/10.1016/j.mseb.2006.08.041

[49] E. Haro-Poniatowski, C. Julien, B. Pecquenard, J. Livage, "Laser-induced structural transformations in MoO_3 investigated by Raman spectroscopy", 13 4 (1998) 1033-1037. https://doi.org/10.1557/JMR.1998.0144

Chapter 5 Conclusions and Future Directions

As shown in this work and the references within, LASL is an effective, straightforward and simple method to produce a big variety of NS, from noble metals and semiconductors, to carbon-based and oxides [1]. Some of the advantages of this technique over laser ablation synthesis in air is that is liquid medium is a relatively safer medium, since it confines the resulting NS, avoiding workplace contamination with aerosols [2]. Contrary to chemical synthesis, this method does not require extra purification procedures to eliminate excess of surfactants and/or reactants [3,4].

However, there are a lot challenges that remain to be solved, some have to do with the technical complexity to study the physical phenomena that involves the L-M interaction, such as plasma, cavitation bubble and shock wave generation, since these phenomena coexist at a given time and space, therefore it is very complex to differentiate how each of them affects the NS formation, composition and structure [5,6].

Another important challenge unsolved is the fact that one cannot have much control over their size of the NS when synthesizing with LASL. Monodisperse NS without compromising colloidal purity has not been achieved [7,8]. Even though, there have been important progress regarding the control of the average size and reduction of the size range by inducing fragmentation and melting with post irradiation of the formed colloids [9].

Furthermore, NS with a broad size range can be synthesized from 1 nm [10] to 10 um [11]. Usually, high intensity pulses generate larger NS [12], but increasing the repetition rate always induces NS fragmentation. Conversely, a relative low laser pulse fluence, induces NS melting and agglomeration, causing merging of agglomerate into

submicron structures [13]. Therefore, it is very difficult to correlate the effects of each mechanism on the NS size [14].

Future work should solve the challenges mention above. For instance, differentiating the effect of plasma, cavitation bubble and shock waves on the NS size and composition, achieving more NS size control, and better understanding of the laser-induced fragmentation and melting process on the post irradiation colloidal solution.

There is a lot of research remaining no only to improve the results of NS synthesized by LASL, but also to expand the understanding of the technique. Some of the investigations I find very interesting for future work are: i) Exploring the potential of the generated NS as PTT agents in *in vitro* studies. ii) Simulating the plasmonic properties of these NS and compare them with the experimental result obtained and iii) Performing LASL with single or few pulses to better understand the influence of the intensity on the NS size and size distribution.

References

[1] D. Zhang, B. Gökce and S. Barcikowski, Laser Synthesis and Processing of Colloids: Fundamentals and Applications, Chem. Rev.2017 1175 3990-4103. https://doi.org/10.1021/acs.chemrev.6b00468

[2] S. Barcikowski, J. Walter, A. Hahn, J. Koch, H. Haloui, T. Herrmann, A. Gatti, A. Picosecond and Femtosecond Laser Machining May Cause Health Risks Related to Nanoparticle Emission. J. Laser Micro/Nanoeng. 2009, 4, 159−164.

[3] R. Leýy, N. Thanh, R. Doty, I. Hussain, R. Nichols, D. Schiffrin, M. Brust and D. Fernig, Rational and Combinatorial Design of Peptide Capping Ligands for Gold Nanoparticles. J. Am. Chem. Soc. 2004, 126, 10076−10084.

[4] I. Ojea-Jimeńez and V. Puntes, Instability of Cationic Gold Nanoparticle Bioconjugates: The Role of Citrate Ions. J. Am. Chem. Soc. 2009, 131, 13320−13327.

[5] J. Dowden, The theory of laser materials processing, 1st ed. Springer series in materials science; 2008.

[6] V. Amendola, M. Meneghetti, What controls the composition and the structure of nanomaterials generated by laser ablation in liquid solution? Phys. Chem. Chem. Phys. 15 (2013) 3027-3046. https://doi10.1039/C2CP42895D.

[7] C. Rehbock, J. Jakobi, L. Gamrad, S. van der Meer, D. Tiedemann, U. Taylor, W. Kues, D. Rath and Barcikowski, S. Current State of Laser Synthesis of Metal and Alloy Nanoparticles as Ligand-Free Reference Materials for Nano- Toxicological Assays. Beilstein J. Nanotechnol. 2014, 5, 1523−1541.

[8] U. Taylor, C. Rehbock, C. Streich, C.; D. Rath, S. Barcikowski, Rational Design of Gold Nanoparticle Toxicology Assays: a Question of Exposure Scenario, Dose and Experimental Setup. Nanomedicine 2014, 9, 1971−1989.

[9] M. Lau, I. Haxhiaj, P. Wagener, R. Intartaglia, F. Brandi, J. Nakamura and S. Barcikowski, Ligand-Free Gold Atom Clusters Adsorbed on Graphene Nano Sheets Generated by Oxidative Laser Fragmentation in Water. Chem. Phys. Lett. 2014, 610−611, 256−260.

[10] H. Castro, V. Souza, J. Scholten, J. Dias, J. Fernandes, F. Rodembusch, R dos Reis, J. Dupont, S. Teixeira and R. Correia, Synthesis and Characterisation of Fluorescent Carbon Nanodots Produced in Ionic Liquids by Laser Ablation. Chem. - Eur. J. 2016, 22, 138−143.

[11] D. Zhang, B. Gökce, C. Notthoff, and S. Barcikowski, Layered Seed-Growth of AgGe Football-like Microspheres via Precursor-Free Picosecond Laser Synthesis in Water. Sci. Rep. 2015, 5, 13661.

[12] S. Besner, A. Kabashin, F. Winnik and M. Meunier, Ultrafast Laser Based "Green" Synthesis of Non-Toxic Nanoparticles in Aqueous Solutions. Appl. Phys. A: Mater. Sci. Process. 2008, 93, 955−959.

[13] T. Tsuji, Y. Higashi, M. Tsuji, H. Fujiwara, Y. Ishikawa and N. Koshizaki, Fabrication of Spherical-Shaped Submicron Particles of ZnO Using Laser-induced Melting of Submicron-sized Source Materials. J. Laser Micro/Nanoeng. 2013, 8, 292−295.

[14] (21) Intartaglia, R.; Bagga, K.; Brandi, F. Study on the Productivity of Silicon Nanoparticles by Picosecond Laser Ablation in Water: towards Gram per Hour Yield. Opt. Express 2014, 22, 3117−3127.